# APPLICATION OF WAVELET-FILTERING TECHNIQUES TO INTERMITTENT TURBULENT AND WALL-PRESSURE EVENTS

## PART II — Detection of Cluster Patterns

Mario J. Casarella, Pablo B. Penafiel and Mark E. Kammeyer
The Catholic University of America

April 1995

# APPLICATION OF WAVELET-FILTERING TECHNIQUES TO INTERMITTENT TURBULENT AND WALL-PRESSURE EVENTS

## PART II — Detection of Cluster Patterns

Mario J. Casarella, Pablo B. Penafiel and Mark E. Kammeyer
The Catholic University of America

April 1995

# REPORT DOCUMENTATION PAGE

Form Approved
OMB No. 0704-0188



| 1. AGENCY USE ONLY (Leave Blank) | 2. REPORT DATE | 3. REPORT TYPE AND DATES COVERED |
|---|---|---|
| | April 26, 1995 | Progress report 11/94 thru 11/95 |

**4. TITLE AND SUBTITLE**
Application of Wavelet-Filtering Techniques to Intermittent Turbulent and Wall Pressure Events.
Part II Detection of Cluster Patterns

**5. FUNDING NUMBERS**
N00014-88-K-0141

**6. AUTHOR(S)**

**7. PERFORMING ORGANIZATION NAME(S) AND ADDRESS(ES)**
The Catholic University of America
Department of Mechanical Engineering
Washington D.C. 20064

**8. PERFORMING ORGANIZATION REPORT NUMBER**

**9. SPONSORING/MONITORING AGENCY NAME(S) AND ADDRESS(ES)**
Office of Naval Research
800 North Quincy St.
Alexandria, VA 22217-5000

**10. SPONSORING/MONITORING AGENCY REPORT NUMBER**

**11. SUPPLEMENTARY NOTES**

**12a. DISTRIBUTION/AVAILABILITY STATEMENT**
Approved for public release; distribution is unlimited.

**12b. DISTRIBUTION CODE**

**13. ABSTRACT (Maximum 200 words)**

## Abstract

Large amplitude wall-pressure events, observed beneath a turbulent boundary layer, appear to be signatures of intermittent organized motions within the turbulent flow. Experimental studies were made investigating this relationship. Part I presented the first phase of this investigation and reported on the results of utilizing time-frequency localization techniques (wavelet transforms) for the detection of these events. The application of wavelet filtering for the analyses of turbulent data was introduced.

This report presents the results of the second phase of the investigation. A wavelet filter was selected based on maintaining the integrity of intermittent near wall burst events. The correlations between individual turbulent flow and wall-pressure events were confirmed using both the original time records and the generated VITA function time records. A Localized Windowed Peak Detection algorithm was developed that detects the groupings of these events. The algorithm detects the temporal locations and durations of the clusters. Correlation and conditional sampling methods were then used to postulate the sequential burst events contained within the individual clusters. Conditional sampling showed a bi-directional relationship between positive wall-pressure events and burst ejections in the near-wall region.

| 14. SUBJECT TERMS | 15. NUMBER OF PAGES |
|---|---|
| wavelet filtering, wall-pressure fluctuations, turbulence time-frequency localization, conditional sampling | 61 |
| | 16. PRICE CODE |

| 17. SECURITY CLASSIFICATION OF REPORT | 18. SECURITY CLASSIFICATION OF THIS PAGE | 19. SECURITY CLASSIFICATION OF ABSTRACT | 20. LIMITATION OF ABSTRACT |
|---|---|---|---|
| UNCLASSIFIED | UNCLASSIFIED | UNCLASSIFIED | UL |

# Contents

## Abstract

Large amplitude wall-pressure events, observed beneath a turbulent boundary layer, appear to be signatures of intermittent organized motions within the turbulent flow. Experimental studies were made investigating this relationship. Part I presented the first phase of this investigation and reported on the results of utilizing time-frequency localization techniques (wavelet transforms) for the detection of these events. The application of wavelet filtering for the analyses of turbulent data was introduced.

This report presents the results of the second phase of the investigation. A wavelet filter was selected based on maintaining the integrity of intermittent near wall burst events. The correlations between individual turbulent flow and wall-pressure events were confirmed using both the original time records and the generated VITA function time records. A Localized Windowed Peak Detection algorithm was developed that detects the groupings of these events. The algorithm detects the temporal locations and durations of the clusters. Correlation and conditional sampling methods were then used to postulate the sequential burst events contained within the individual clusters. Conditional sampling showed a bi-directional relationship between positive wall-pressure events and burst ejections in the near-wall region.

# Chapter 1

# INTRODUCTION

## 1.1 Background

It has been widely postulated that large amplitude wall-pressure events can be used as a non-intrusive observation of the passage of organized flow structures. These organized motions are proposed to be the primary mechanism for the production of turbulence (cf. [1]). It is speculated that the temporal localization of these surface events could be used for the active control of turbulent wall flows.

The pressure fluctuations beneath a turbulent boundary layer are the integral effects of *active* (turbulence producing) and *passive* (high kinetic energy) flow structures throughout the boundary layer. Bradshaw (cf. [21]) presents an enlightening discussion on the concept of *inactive* (passive) motions. These are defined as motions generated by eddies in the outer layer which cause secondary effects on pressure fluctuations and turbulence in the near-wall region. Signal detection techniques on the temporal records of the pressure are required to discriminate between the two contributions. In the context of this paper, the pressure fluctuations of the passive or inactive motions will be considered as noise contamination on the pressure signatures.

Previous work by Farabee and Casarella (cf. [2]) had shown that turbulent sources of the wall pressure spectrum can be attributed to flow activities at distinct locations across the boundary layer. They concluded that the inner layer is characterized by high frequency turbulent motions while the outer layer is characterized by low frequency structures. It is widely believed that

the near-wall (active) structures can spatially extend to the overlap region and are thus not limited to a distinct spatial location.

A more tractable approach is to examine the intermittent large-amplitude pressure events at the wall. These appear to be the footprint of the bursting process associated with the near-wall turbulent production mechanism (cf. [3]). Extensive work has been done using a range of schemes for the simultaneous detection of intermittent large-amplitude turbulent and wall-pressure events (cf. [4, 5, 7]). Conditional sampling techniques are often used and these include detection algorithms based on peak amplitudes and VITA algorithms (cf. [6]).

By ensemble averaging the collection of detected events, a correlation can be observed between turbulent events and peak pressure events. These methods are not very effective for examining a cluster of events nor for evaluating the time delay between occurring events. A new approach for detection of turbulent clusters will be proposed based on the Localized Windowed Peak Detection Algorithm. This will be discussed in detail in the report.

## 1.2 Experimental Arrangement

New equilibrium flow data were acquired during the past year using an improved data acquisition system [Kammeyer, 1995]. In addition, data were obtained for a non-equilibrium flow configuration. These databases were analyzed using the techniques presented in this report. A brief description of the experimental arrangement used to obtain these data will be presented.

The experiments were performed in the Low Noise Flow Facility at Catholic University. The facility was constructed specifically for making acoustic measurements of wall pressure beneath turbulent flows. A complete description can be found in [2].

Two flows were studied: an equilibrium turbulent boundary layer (ETBL); and a disturbed turbulent boundary layer (DTBL). The instrumentation used included sensors to monitor the state of the wind tunnel, two microphones for the measurement of the fluctuating wall pressure, and single-component hot wire and two-component hot film anemometers for the measurement of fluctuating streamwise and wall-normal velocities.

The boundary layers studied in this investigation were formed on one wall of the wind tunnel. The measurements for the equilibrium flow were

Table 1.1: Nominal boundary layer properties and measurement resolutions.

| | Equilibrium TBL | | Disturbed TBL | |
|---|---|---|---|---|
| | Single Wire | X-wire | Single wire | X-wire |
| $U_e$ | 14.79 m/s | 16.13 m/s | 13.74 m/s | 16.18 m/s |
| $u_\tau/U_e$ | 0.040 | 0.040 | 0.023 | 0.028 |
| $\delta$ | 2.72 cm | 2.95 cm | 4.05 cm | 4.30 cm |
| $\delta^+$ | 1064 | 1202 | 836 | 1255 |
| $Re_\theta$ | 3045 | 3358 | 4599 | 5397 |
| $H$ | 1.3872 | 1.4193 | 1.8492 | 1.7393 |
| $G$ | 6.9309 | 7.4083 | 19.7216 | 15.3768 |
| $C_f$ | 0.00324 | 0.00318 | 0.001084 | 0.001528 |
| $l_\nu = \nu/u_\tau$ | 25.6 $\mu$m | 24.6 $\mu$m | 48.4 $\mu$m | 34.2 $\mu$m |
| $t_\nu = \nu/u_\tau^2$ | 42.9 $\mu$s | 38.2 $\mu$s | 151.3 $\mu$s | 76.5 $\mu$s |
| $l_{wire}$ | 1.27 mm | 1.0 mm | 1.27 mm | 1.0 mm |
| | $(50l_\nu)$ | $(41l_\nu)$ | $(26l_\nu)$ | $(29l_\nu)$ |
| $d_{mic}$ | 0.79 mm | 0.79 mm | 0.79 mm | 0.79 mm |
| | $(31l_\nu)$ | $(32l_\nu)$ | $(16l_\nu)$ | $(23l_\nu)$ |
| $\Delta t_s$ | 30.5 $\mu$s | 30.5 $\mu$s | 30.5 $\mu$s | 30.5 $\mu$s |
| | $(0.71t_\nu)$ | $(0.80t_\nu)$ | $(0.20t_\nu)$ | $(0.40t_\nu)$ |

obtained on the tunnel center line at approximately 1.4 m downstream of the test section entrance. At this location, the boundary layer is approximately 3 cm thick for a tunnel speed of 16 m/s. The disturbed turbulent boundary layer approximated the flow over an aft-facing step. This was accomplished by installing a ramp of length 0.51 m on the tunnel wall ending 0.13 m upstream of the measurement station. The step height, $h$, was 1.5 cm. The ramp spanned the width of the tunnel, and the leading edge was faired into the tunnel wall using modeling clay. The characteristics of the resulting boundary layers are presented in table 1.1.

Wall pressure measurements were made simultaneously using two microphones, identified as $p_1$ and $p_2$. Microphone $p_1$ was mounted at the primary measurement station beneath the hot-wire probe, while microphone $p_2$ was mounted 1.27 cm upstream of $p_1$. The microphones were Brüel and Kjær $\frac{1}{8}$ inch condenser microphones (model 4138). Figure 1.1 shows a schematic of the instrumentation and data acquisition systems. Only one microphone is illustrated for clarity.

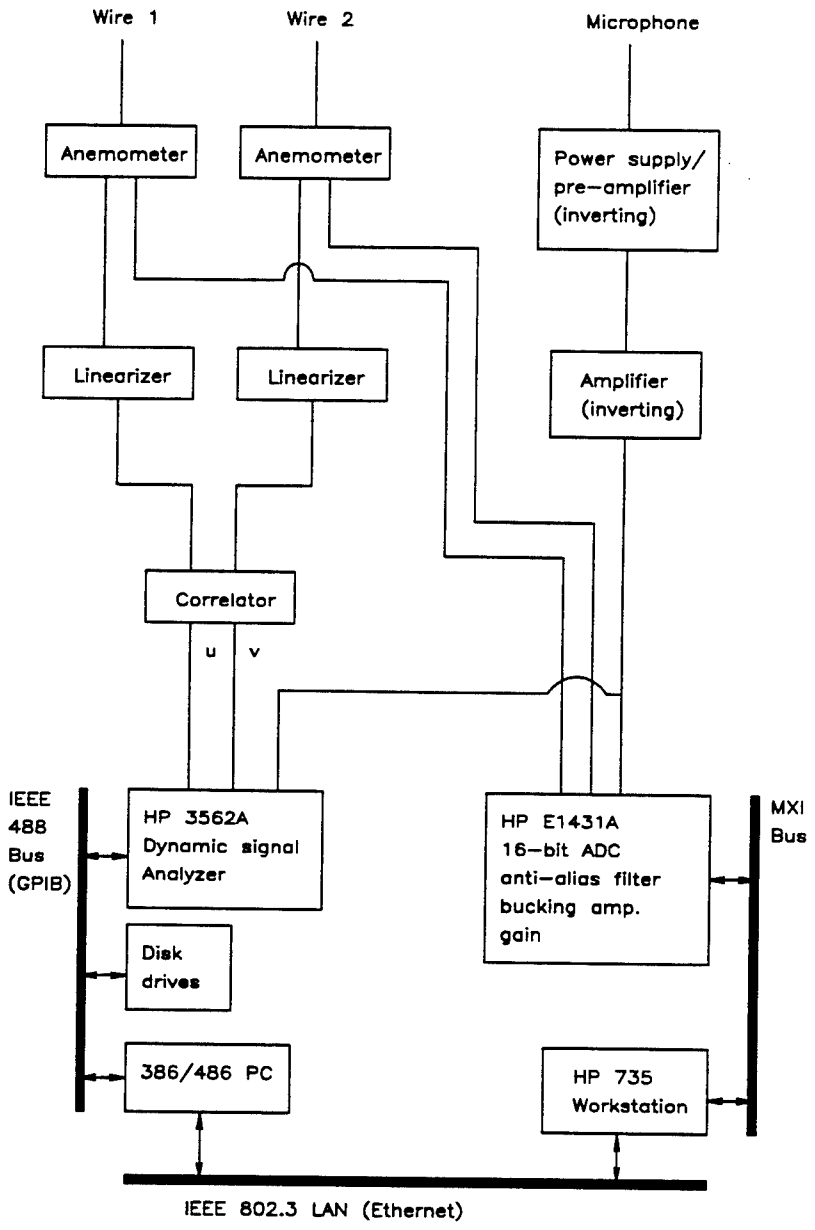


Figure 1.1: Schematic of instrumentation and data acquisition systems. Only one microphone system is shown for clarity.

Digital data were acquired on a system based on the VMEbus Extensions for Instrumentation (VXIbus or VXI) specification. The VXI system uses a mainframe chassis with slots to hold modular instruments on plug-in boards. The specific system was manufactured by the Hewlett Packard Company. An HP C-size mainframe (E1401A) provided the VXI backplane, cooling, power, and current requirements. Digitization was performed by an Eight Channel VXI Input Module (HP-E1431A). This module was chosen for its high sampling rates, built-in signal conditioning, and high resolution, 16-bit, analog-to-digital converter. The module featured simultaneous sampling on up to eight differential input channels. Sampling rates were selectable in powers of two from 1 to 65536 Hz, with alias protection provided internally by anti-alias filters.

The system was controlled by an HP model 735 workstation via Multisystem eXtension Interface bus (MXIbus), using the VXI-to-MXI interface module (HP-E1482B) in the mainframe and the EISA/ISA-to-MXI interface card (HP E1439I) in the workstation. Data were acquired from the A/D module directly to the HP 735 main memory. A maximum of four channels were used simultaneously to acquire data from the two microphones and the two-component hot-wire.

Data were collected for two different flows: an equilibrium turbulent boundary layer (ETBL) and a disturbed turbulent boundary layer (DTBL). For each of these flows, a single-wire survey and several X-wire surveys were performed. For each single wire survey, the streamwise velocity $U$, and the wall pressure at two x-locations $p_1$ and $p_2$, were measured at each of 22 or 23 y-locations across the boundary layer. Several X-wire surveys were required in order to obtain the desired cross spectral data pairs: $U$-$V$, $U$-$p_1$, and $V$-$p_1$.

In addition to controlling the VXI data system, the HP workstation performed engineering unit conversions and all subsequent analyses of the digitized data. All computations and graphics were performed using MATLAB™ scientific software running under the HP-UX operating system. The raw binary time series data were read into MATLAB . The data were then digitally filtered to remove unwanted electrical and acoustic noise. This was done using a 5th-order high-pass Butterworth filter with a cutoff frequency of 100 Hz. The filter was applied both forwards and backwards in order to eliminate phase lags. To account for end effects, 500 points were deleted from both ends of the filtered record. The data were then stored in MATLAB binary format for further processing.

## 1.3 Overview of the Investigation

The $u$, $v$ and $p$ time records acquired from the experiment can be assumed to be random processes of the form

$$u(t) = u_s(t) + u_n(t) \quad (1.1)$$
$$v(t) = v_s(t) + v_n(t) \quad (1.2)$$
$$p(t) = p_s(t) + p_n(t) \quad (1.3)$$

where $u_s(t)$, $v_s(t)$ and $p_s(t)$ are due to active structures in the turbulent flow, and $u_n(t)$, $v_n(t)$ and $p_n(t)$ are assumed to be noise (in general, non-gaussian). It is postulated that $u_s$ and $v_s$ are highly correlated and represent the distinct features of organized structures. In turn, $p_s(t)$ represents the unique signatures of these intermittent flow events.

In the first phase of this investigation, a filtering technique, based on orthogonal wavelet expansion, was proposed to isolate the signal from the noise in the time records. A weighting scheme that allowed a systematic selection of the coefficients was introduced. The criterion for selection was to preserve the shape of the large amplitude turbulent events.

This report contains the findings of the second phase of the investigation which is directed at designing a filter for this application and utilizing it in a detection algorithm.

The specific tasks can be summarized as:

1. Select wavelet filters that preserve the distinct features of both the turbulent burst events and the large amplitude wall-pressure events.

2. Develop an algorithm that detects the temporal localization of these intermittent events.

3. Compute the correlation between the flow structure and wall-pressure events utilizing the combined filtering and detection algorithms.

4. Create an algorithm that can detect and identify the cluster pattern for both the burst and wall-pressure events while maintaining their phase relations.

This report will focus on the results for the equilibrium database. The dissertation research of Kammeyer (1995) will extend the investigation to the disturbed (non-equilibrium) flow for which the noise (passive structures) has significantly higher levels. A comparison of the results between equilibrium and disturbed flow will be presented in the dissertation. It should be noted that the filter design and detection algorithms to be discussed in this report were chosen, to a large extent, based on the more severe case of a disturbed flow. The equilibrium flow was considered the generic configuration that can be used for comparative evaluation.

# Chapter 2

# DESIGN OF THE WAVELET FILTER

In the first phase of this investigation, Daubechies D8 wavelets were shown to be an appropriate choice for the representation of the time records. Results were presented that displayed the characteristics of the D8 wavelet expansion and the ability to design a filter by weighting the coefficients. A criterion must be now established for the selection of the *best filter* using this orthonormal basis.

## 2.1 Power Distribution in Wavelet Expansion

It is widely postulated that turbulence measurements in the near wall region ($y/\delta \leq 0.2$) contain two types of organized motions: The *active structures* which are, for the most part, reflected in the high frequency range; and some *inactive structures*, including the induced irrotational motions concentrated in the low frequency range (cf. [2, 5, 7, 22]). A filtering scheme attempts to separate these signals as stated in equations 1.1, 1.2 and 1.3.

An explicit classification of the spectral ranges associated with data from the inner and outer regions of the boundary layer had been established by Farabee and Casarella (cf. [2]) and is shown in table 2.1. The results were obtained by collapsing wall-pressure data over a range of flow-speeds based on the inner and outer scaling relationships. It was deduced that the high-

Table 2.1: Spectral regions based on scaling laws for equilibrium data

| Spectral Range | $w\delta/u_\tau$ | $f$ (Hz) | Rows of Wavelet Expansion |
|---|---|---|---|
| mid | $5 \leq w\delta/u_\tau \leq 100$ | 200–360 | $m = 5, 6, 7$ |
| overlap | $100 \leq w\delta/u_\tau \leq 0.30R_\tau$ | 360–1200 | $m = 3, 4, 5$ |
| high | $0.30R_\tau \leq w\delta/u_\tau$ | $\geq 1200$ | $m = 2, 3, 4$ |

Table 2.2: Center frequency of D8 wavelets

| $m$ | $f_c$/ (Hz) |
|---|---|
| 2 | 2180 |
| 3 | 1090 |
| 4 | 545 |
| 5 | 272 |
| 6 | 136 |
| 7 | 68 |

frequency range is dominated by turbulence structures in the near-wall region, the overlap range reflects activities in the log-law region, and the mid-frequency range reflects activities in the outer-layer. It should be noted that the induced irrotational motion has spectral content in the mid-frequency range but its structure extends across the complete boundary layer. Therefore, the near-wall measurements also contain these motions as previously stated.

Table 2.1 also lists the rows of the D8 wavelet expansion associated with each frequency range. Table 2.2 tabulates the center frequency for the wavelets in the respective rows. Wavelets in rows $m = 2, 3, 4$ have frequency bands in the high-frequency range while wavelets in rows $m = 5, 6, 7$ have bands in the mid-frequency range. The *induced irrotational motion* covers the frequency range ($108 < f < 252$ Hz) and these are contained in wavelets with $m = 5, 6, 7$.

Figures 2.1 and 2.2 show the wavelet power versus $m$ for $u(t)$ and $v(t)$ at locations $y/\delta = 0.025$, 0.250 and 0.926. These locations reflect the near wall, log-law region and outer edge of the turbulent boundary layer, respectively. The $u(t)$ results are consistent with the conjecture that the near wall region is dominated by high frequency turbulence while the $v(t)$ does not display any apparent trend. No clear pattern can be deduced from the wavelet power.

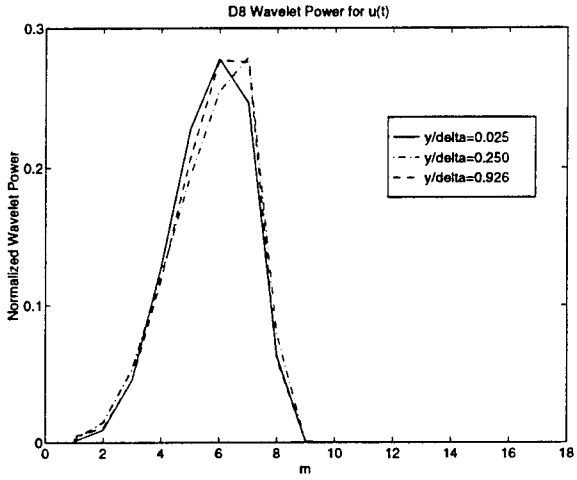


Figure 2.1: D8 Wavelet Power versus $m$ for $u(t)$ at $y/\delta = 0.025$, 0.250 and 0.926.

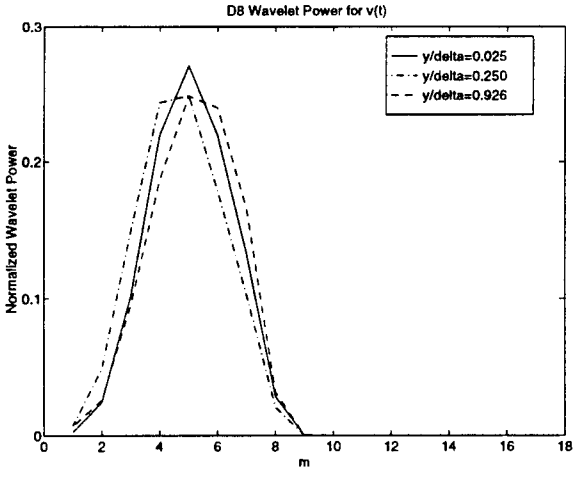


Figure 2.2: D8 Wavelet Power versus $m$ for $v(t)$ at $y/\delta = 0.025$, 0.250 and 0.926.

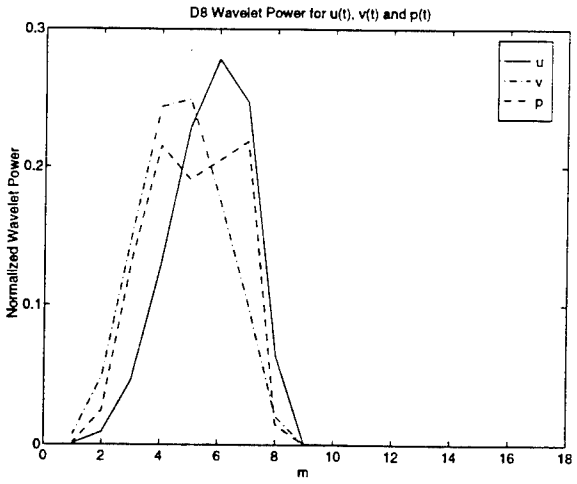


Figure 2.3: D8 Wavelet Power versus $m$ for $u(t)$, $v(t)$ and $p(t)$ at $y/\delta = 0.025$.

It should be noted that at the near-wall location ($y/\delta = 0.08$), the $v(t)$ signal contains more high-frequency content than $u(t)$ and thus significantly more energy in wavelets with $m = 2, 3$ and 4. This is shown in figure 2.3, which also includes the wavelet power for the $p(t)$ time record. The $p(t)$ signal contains the same high frequency content of the $v(t)$ time record, but also includes another peak in the low frequency range. This secondary peak is due to noise contamination by the traverse system and should be eliminated by the filter. This was confirmed by comparing the $p(t)$ records with and without the installation of the traverse system.

A filtering scheme for the near-wall measurements should attempt to reduce the coefficients in those rows dominated by lower frequency content. As a first attempt at designing a wavelet filter, extensive computations were made utilizing three weighting schemes $w(m) = 2^{-\alpha m}$ previously discussed in Part I of this investigation. The techniques were applied simultaneously to $u(t)$, $v(t)$ and $p(t)$ time records at several locations across the turbulent boundary layer. The high-pass filtering scheme with the weighting $w(m) = w^{-m}$ ($\alpha = 1$) shown in figures 2.4 and 2.5 was a crude attempt in this direction. Extensive computations were made with these filters and the results did not show any improvement in detection of turbulent events. A more refined method of weighting $w(m)$ is required with separate filters for the $u(t)$, $v(t)$ and $p(t)$ signals. In addition, the filtering should be directed

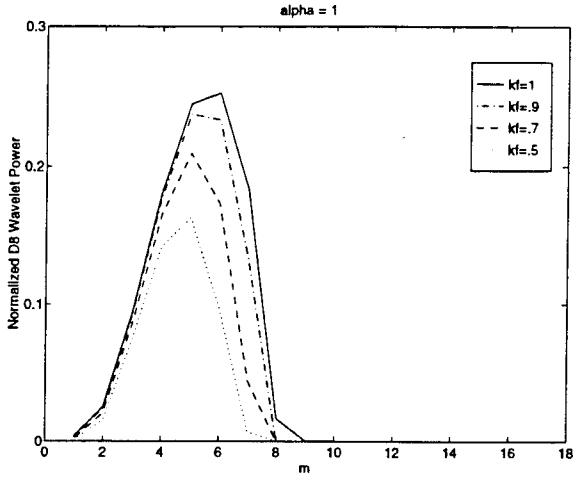


Figure 2.4: Normalized D8 Wavelet Power of $u(t)$ for $w(m) = 2^{-m}$ ($\alpha = 1$) and $k_f = 1, .9, .7$ and $.5$

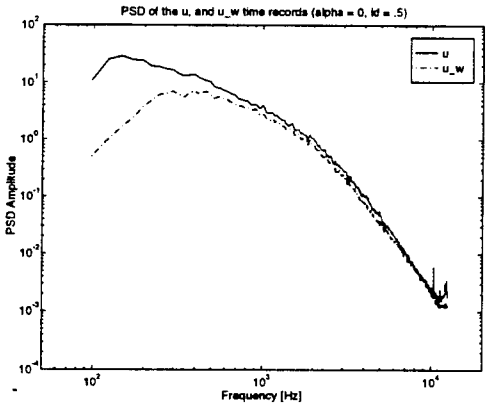


Figure 2.5: PSD of $u(t)$ (solid) and $u_w(t)$ (dashed) for $k_f = .5$ and $w(m) = 2^{-m}$ ($\alpha = 1$)

at examining the integrity of burst events rather than the $u(t)$ and $v(t)$ time records.

## 2.2 Selection of a Wavelet Filter

The identification of the passage of organized motions in the near-wall region of the boundary layer by means of observing the $u(t)$ and $v(t)$ time records at a fixed location is the primary task. Much controversy exists over the spatial and temporal features of these structures. However, it has been clearly established that the inherent characteristic of this motion is the bursting process. This process consists of intermittent periods of ejections from the wall into the outer region and sweeps from the outer regions towards the wall. These burst events are referred to as 'active' motions since they are directly related to the Reynolds stress $\overline{uv}$ and the turbulent production mechanism.

It has not been resolved as to what pattern or combination of these burst events are associated with the same large-scale flow structure. It appears that a typical pattern consists of two or more ejections combined with several sweeps. A recent study by Kaftori, Hetsroni and Banarjee (cf. [17, 18]) proposed that these active motions are part of a funnel-shaped vortical structure in the wall layer.

The regions of high Reynolds stress are traditionally used to identify the locations of active motions. More specifically, the Q2 (ejections) and Q4 (sweeps) events located in the second and fourth quadrant of the $u$-$v$ plane are of prime importance. It is the cluster or group of these 'active' events that will be used to define the signature of large-scale organized motions. A filtering technique is required to clearly isolate these patterns in the time records and identify their passage through their footprint in the wall pressure time records.

The $u$, $v$ and $p$ random processes were modeled in equations 1.1, 1.2 and 1.3. The primary quantity under scrutiny, the $uv(t)$ time record, is given by

$$\begin{aligned} uv(t) &= [u_s(t) + u_n(t)][v_s(t) + v_n(t)] \\ &= u_s(t)v_s(t) + u_s(t)v_n(t) + v_s(t)u_n(t) + u_n(t)v_n(t) \quad . \end{aligned} \tag{2.1}$$

It should be noted that the noise can consist of outer flow structures

for which $u_n$ and $v_n$ are correlated, for example, the induced irrotational motions.

The objectives for filtering the temporal records of $u$, $v$ and $p$ are:

- To maintain the cluster of high-amplitude Q2 and Q4 events while filtering the extraneous low-frequency and high-frequency noise.
- To isolate large amplitude wall-pressure events that are associated with the cluster of $uv$ events.

The task is to design a wavelet filter that extracts $u_s(t)$, $v_s(t)$ and $p_s(t)$ from the signal. More explicitly, the task is to design a weighting scheme $w(m)$ by means of a trial and error procedure that meets the stated objectives.

An improved weighting scheme can be developed by selectively maintaining some rows and eliminating others from the wavelet expansion. That is,

$$w(m) = \begin{cases} 1 & \text{for } m = m_1, m_2 \ldots m_r \\ 0 & \text{otherwise} \end{cases} \quad \text{where} \quad \begin{cases} 1 \leq m < \mathrm{N} \\ 1 \leq r < \mathrm{N} \end{cases} \tag{2.2}$$

An additional refinement, that allows significant data compression, can be incorporated in the algorithm. This is performed by first sorting in descending order all the coefficients in the retained $m^{th}$ row and then select only the large amplitude coefficients within a row until a fraction $k_f(m)$ of the total energy in that row is preserved. $k_f(m)$ will be called the filtering parameter of the $m^{th}$ row.

A wavelet filter was selected after extensive studies using various wavelet bases; a range of weighting functions $w(m)$ for the choice of rows; and numerous values of the fraction of the power $k_f(m)$ preserved in each row. This will be denoted as the F2 filter.

The Daubechies Extremal Phase implemented with FIR filters having 8 coefficients (D8) proved to be an appropriate wavelet to represent the time records as shown in Part I of this investigation. The filter F2 is based on the D8 wavelet expansion.

Even though $u(t)$ and $v(t)$ have slightly different spectral contents, the same weighting function is applied to both time records through the F2 filter. Only rows with $m = 3, 4$ and 5 are preserved in the wavelet expansion.

Table 2.3: Characteristics of the F2 Wavelet Filter

| D8 discrete orthogonal wavelet expansion |
|---|
| $u(t)$ time record |
| Retain only rows $m = 3, 4, 5$ with $k_f(3) = k_f(4) = k_f(5) = 0.99$ |
| $v(t)$ time record |
| Retain only rows $m = 3, 4, 5$ with $k_f(3) = k_f(4) = k_f(5) = 0.99$ |
| $p(t)$ time record |
| Retain only rows $m = 2, 3, 4$ with $k_f(2) = k_f(3) = 0.99, k_f(4) = 0.60$ |

The values of $k_f(m) = 0.99$ for $m = 3, 4$ and 5 were selected primarily for compression of the data. No significant improvement was found with lower values.

Since we are trying to correlate the wall-pressure events with the $uv(t)$ time records, the high-frequency range of the pressure records must be maintained. Therefore rows $m = 2, 3,$ and 4 were maintained in the F2 filter for the $p(t)$ time records. The values of $k_f(m) = 0.99$ were selected for rows $m = 2$ and 3. For row $m = 4$, $k_f(4) = 0.60$ was found to be the best choice. This is not surprising because in the frequency range ($150 \leq f \leq 400$ Hz) the traverse system has caused some contamination in the pressure record.

The filter F2 is completely described in table 2.3.

The application of the F2 filtering scheme to the $u$, $v$, and $p$ records produces the filtered sequences which will be denoted by $u_w(t)$, $v_w(t)$ and $p_w(t)$ and these results are shown in figure 2.6 for $y^+ = 30.9$. The effects of filtering these time records can be seen in the corresponding wavelet power and power spectral density. These are shown in figures 2.7, 2.8 , 2.9, and 2.10, 2.11, 2.12, respectively.

The plots of the PSD's of the filtered signals show that the effects of filtering are more severe in the $p(t)$ record. This is consistent with the filter selection criterion. It will be shown that in spite of this filtering, the essential features of the pressure events, particularly their location, will be preserved. Karangelen (1991) investigated the spectral content of the large amplitude pressure events. In her investigation, the pressure events were individually detected, gaussian windowed and fourier transformed. The spectrum was obtained by averaging the collection of spectra for the individual events. This was done over a range of flow speeds. The spectral region obtained in

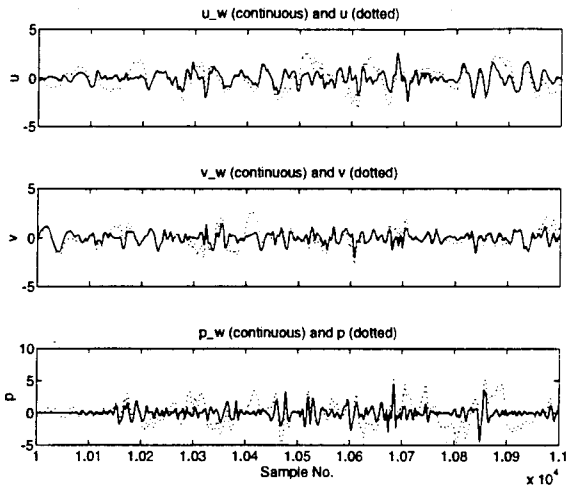


Figure 2.6: Sections of $u_w(t)$, $v_w(t)$, and $p_w(t)$ for $y^+ = 30.9$.

her investigation is consistent with the spectral range shown for the filtered data in figure 2.12.

The essential objective for filtering the $u$, $v$ and $p$ temporal records was to isolate the high-amplitude turbulent and wall-pressure events. Sections of simultaneous $uv(t)$ and $p(t)$ time records, containing 1000 sampled points, are shown in figures 2.13 and 2.14. The filtered and unfiltered sequences shown in this figures have been normalized with respect to their respective RMS values. It appears that filtering helps to isolate the high-amplitude events, particularly for the wall-pressure events.

Peak detection of Q events, with various thresholds H, was performed in both filtered and unfiltered sequences. Figures 2.15 and 2.16 show the location in the $uv$ plane of the peaks of all Q events in the filtered and unfiltered time records for H=1. These results display only the peak value of each detected event rather than all the values that exceed the threshold within each event. This allows the display of the total number of events within the time record. The number of events in each quadrant of the $uv$ plane for H $= 1, 2$ and 3 are tabulated in table 2.4.

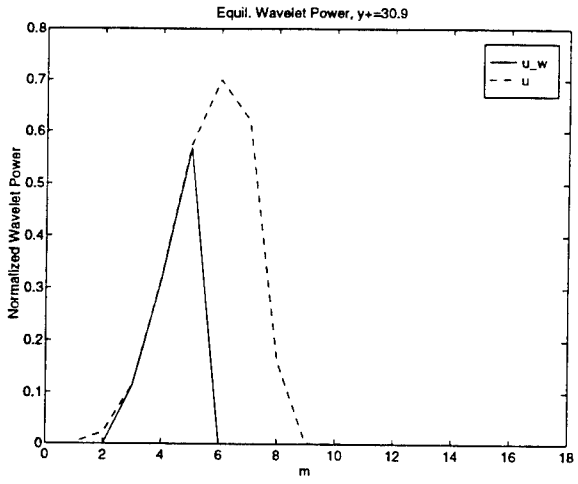


Figure 2.7: Normalized D8 Wavelet Power for the unfiltered $u(t)$ and F2 filtered $u_w(t)$ time records.

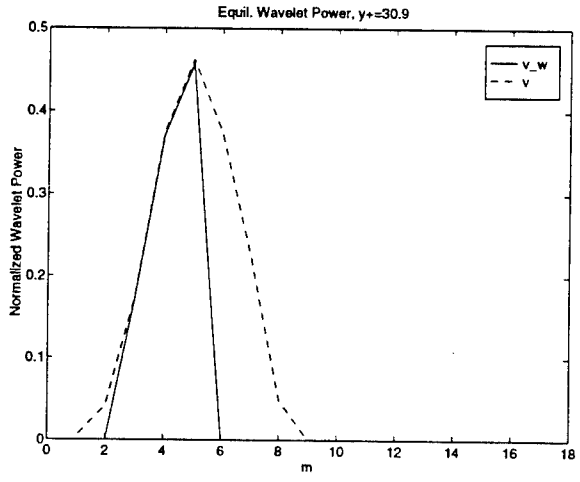


Figure 2.8: Normalized D8 Wavelet Power for the unfiltered $v(t)$ and F2 filtered $v_w(t)$ time records.

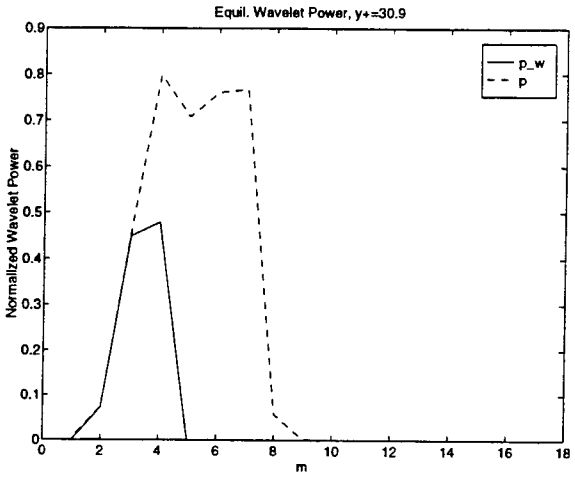


Figure 2.9: Normalized D8 Wavelet Power for the unfiltered $p(t)$ and F2 filtered $p_w(t)$ time records.

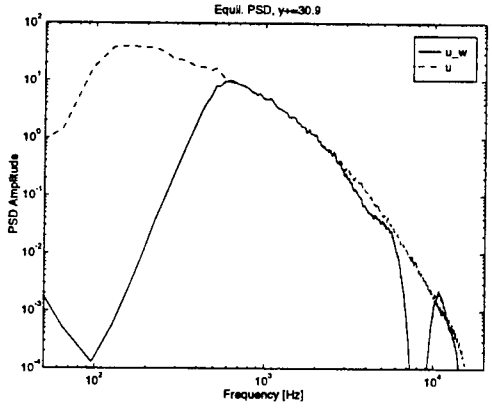


Figure 2.10: PSD of the unfiltered $u(t)$ and F2 filtered $u_w(t)$ time records.

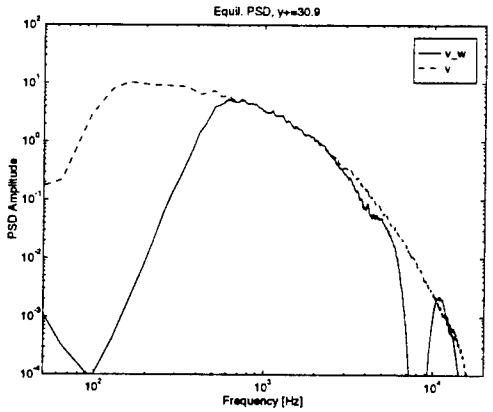


Figure 2.11: PSD of the unfiltered $v(t)$ and F2 filtered $v_w(t)$ time records.

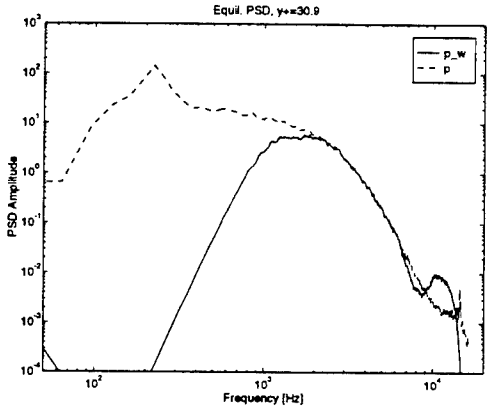


Figure 2.12: PSD of the unfiltered $p(t)$ and F2 filtered $p_w(t)$ time records.

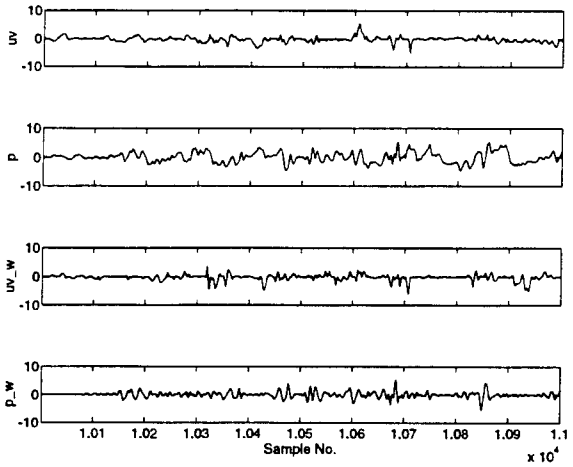


Figure 2.13: Sections of $uv(t)$, $p(t)$ , $uv_w(t)$ and $p_w(t)$ for 1000 samples.

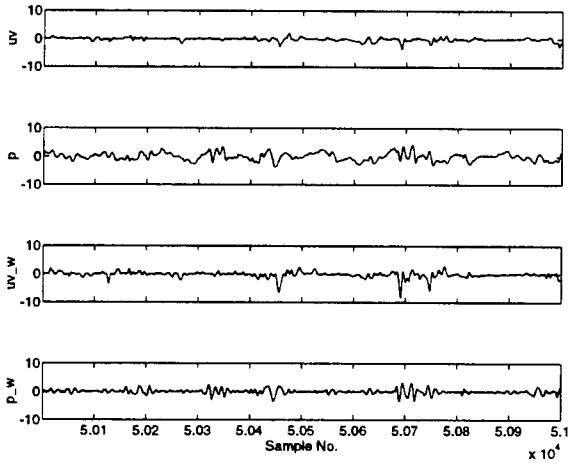


Figure 2.14: Sections of $uv(t)$, $p(t)$ , $uv_w(t)$ and $p_w(t)$ for 1000 samples.

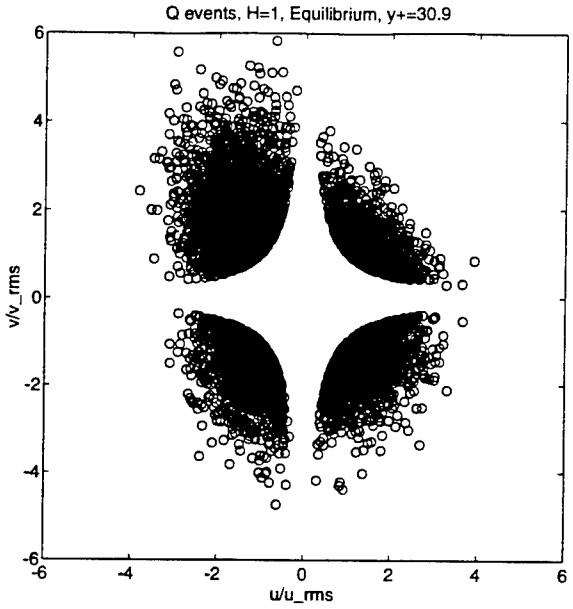


Figure 2.15: Peak value of Q events in the $uv$ plane for threshold H = 1 and unfiltered data.

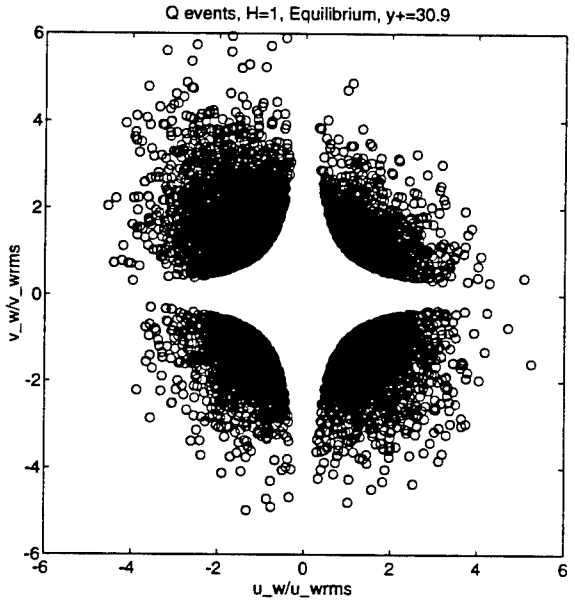


Figure 2.16: Peak value of Q events in the $uv$ plane for threshold H = 1 and filtered data.

Table 2.4: Number of Q events for various thresholds H

| $H$ | $Q_1$ | $Q_2$ | $Q_3$ | $Q_4$ |
|---|---|---|---|---|
| unfiltered | | | | |
| 1 | 1530 | 3508 | 2127 | 2513 |
| 2 | 345 | 2052 | 724 | 768 |
| 3 | 73 | 1197 | 256 | 261 |
| filtered | | | | |
| 1 | 1702 | 3441 | 2080 | 2709 |
| 2 | 481 | 1852 | 729 | 1145 |
| 3 | 190 | 1071 | 287 | 542 |

# Chapter 3

# CORRELATION OF TEMPORAL RECORDS

## 3.1 Estimation of Convection Velocity

The experimental arrangement discussed earlier included the measurements of the wall pressure events at two streamwise locations with a separation distance of $\Delta x^+ = 516$ (1/2 inch). Pressure data were simultaneously collected at both locations. Samples of the time record for both the filtered and unfiltered data are shown in figure 3.1.

These data can be used to compute the time delay between occurring pressure events. This quantity will be used to estimate the convection velocity of the organized motion. For this purpose, a localized correlation function between $p_1(t)$ and $p_2(t)$ was formulated based on dividing the total time record into $n$ windows of size $T_c$ and then performing the correlation between pairs of windows.

$$R_{p_i}(\tau, T_c) = E\{p1_i(t_0), p2_i(t_0 + \tau)\}, \quad i = 1, \ldots, n \ . \tag{3.1}$$

These $n$ correlation functions were then ensemble averaged to display the localized correlation function $R_p(\tau, T_c)$. For the processed data to be presented, $T_c = 2048$ data points and $n = 128$ windows are assumed unless noted. The results for unfiltered and filtered data are shown in figures 3.2 and 3.3, respectively. The locations of positive peaks of the correlation functions were found to be independent of the position of the hot-wire system.

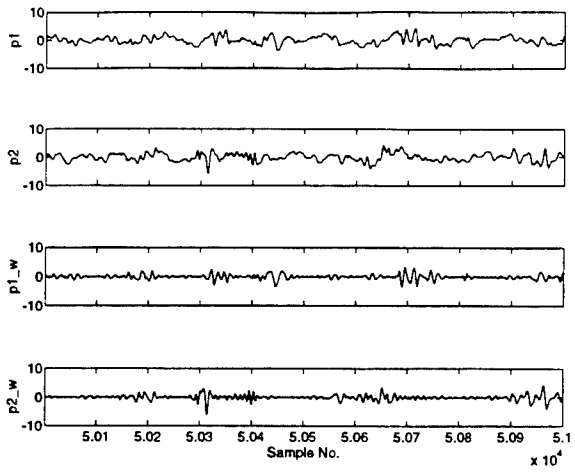


Figure 3.1: Sections of $p_1(t)$, $p_2(t)$, $p_{1_w}(t)$ and $p_{2_w}(t)$.

The calculations for the convection velocities using unfiltered and filtered data are $U_c^+ = 17.4$ and $U_c^+ = 16.5$, respectively. Based on the mean flow profile, this corresponds to turbulent structures located in the log-law region of the boundary layer.

## 3.2 Correlation between Turbulence and Wall-Pressure Time Records

The global correlation function between turbulence and wall-pressure time records have shown some causality between the wall-pressure and turbulent motions and these were presented in Part I of this report (cf. [23]). However, the detailed aspects of the phase relationship between simultaneous events were not clearly observed. In a similar manner to that discussed for the two pressure records, a localized correlation function between the $uv(t)$ and wall-pressure time records is defined as

$$R_{b_i}(\tau, T_c) = E\{uv_i(t_0), p_i(t_0 + \tau)\}, \quad i = 1, \ldots, n \ . \tag{3.2}$$

The $n$ correlation functions are also ensemble averaged to display the localized correlation function $R_b(\tau, T_c)$. Figures 3.4 and 3.5 show the results for unfiltered and filtered records, respectively.

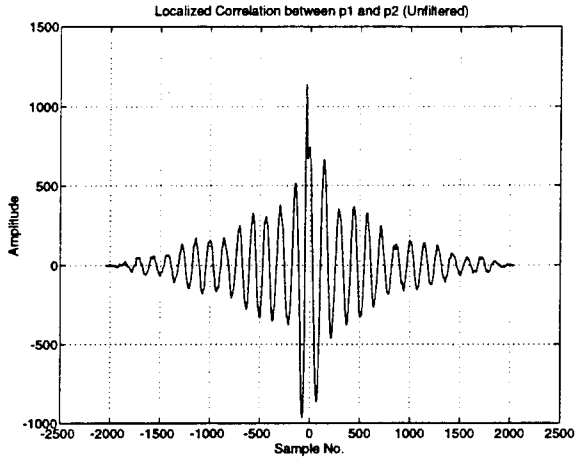


Figure 3.2: Localized correlation function between $p_1(t)$ and $p_2(t)$ for hot-wire system at $y^+ = 30.9$.

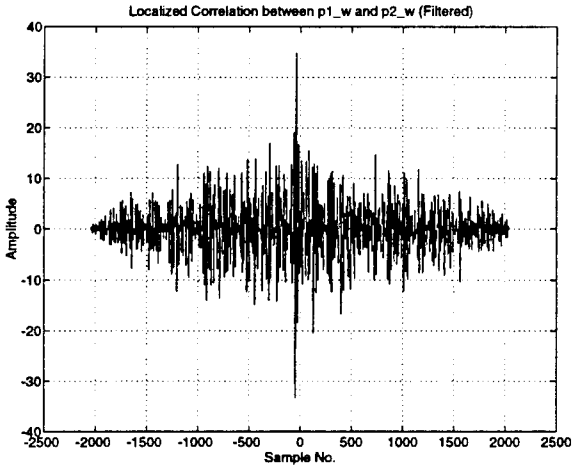


Figure 3.3: Localized correlation function between $p_{1_w}(t)$ and $p_{2_w}(t)$ for hot-wire system at $y^+ = 30.9$.

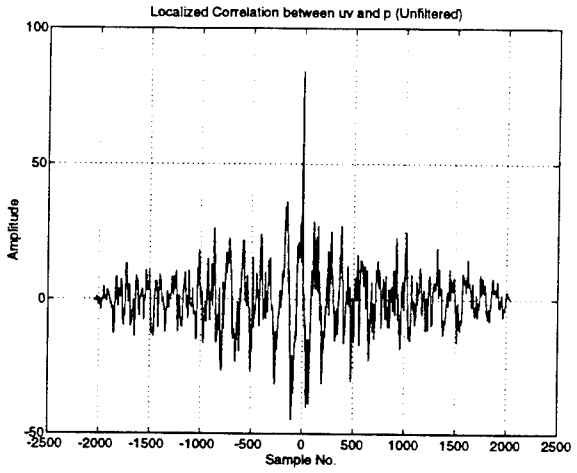


Figure 3.4: Localized correlation function between $uv(t)$ and $p(t)$ for hot-wire system at $y^+ = 30.9$.

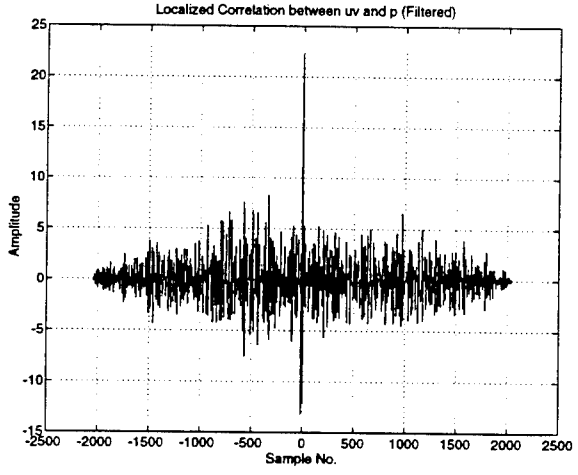


Figure 3.5: Localized correlation function between $uv_w(t)$ and $p_w(t)$ for hot-wire system at $y^+ = 30.9$.

The data shown in figures 3.4 and 3.5 were obtained at a near wall location of $y^+ = 30.9$. A basic question is: Does the correlation extend itself across the boundary layer?. Computations of the correlation function were made at several locations across the boundary-layer with the unfiltered and filtered records. The unfiltered data showed some correlation that extended to the log-law region. The correlations of the filtered data only exist in the near-wall region. This is to be expected since the turbulence and pressure records were severely filtered in the mid- and overlap spectral ranges. These results are inconclusive as to the spatial extent of the organized structures. In the next section this question will be re-examined using an algorithm that attempts to directly correlate the intermittent burst events with large amplitude wall pressure events.

# Chapter 4

# CORRELATION OF CLUSTERS OF EVENTS

## 4.1 VITA Function Detection

In the earlier investigation, the filtered results were examined using traditional event detection and conditional sampling methods. The VITA (Variable-Interval Time-Average) method along with a slope criterion was applied to the $u(t)$ time record to detect the burst event locations. Ensemble averaging performed at these locations produced patterns of $Q_2$ and $Q_4$ events. They appeared to occur in paired combinations at the axis crossing of the VITA events (cf. [7, 16]). However, this method has its shortcomings. For example, it cannot be used to detect the grouping of burst events. These cluster patterns are of primary importance because they appear to be the signature of organized flow structures.

The VITA method is successful in finding localized events in the time record that are characterized by rapid relative changes in the instantaneous power of the signal. For a time record $\phi(t)$ the corresponding VITA function can be expressed as

$$\phi_v(t_0, T_v) = \frac{1}{T_v} \int_{t_0 - \frac{T_v}{2}}^{t_0 + \frac{T_v}{2}} \phi^2(t_0 + \tau) d\tau - \left\{ \frac{1}{T_v} \int_{t_0 - \frac{T_v}{2}}^{t_0 + \frac{T_v}{2}} \phi(t_0 + \tau) d\tau \right\}^2 . \tag{4.1}$$

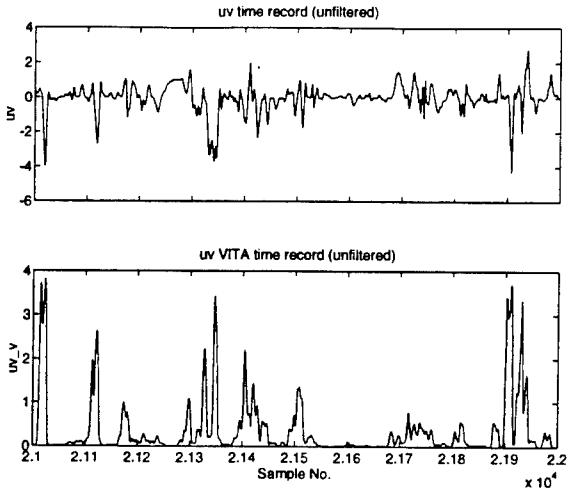


Figure 4.1: Sections of $uv(t)$ and $uv_v(t)$ (unfiltered) for $y+ = 30.9$.

The VITA function $\phi_v(t_0, T_v)$ represents a measure of the local variance of the $\phi(t)$ time record over the time interval $T_v$. The time $t_0$ is the localized time under examination. The time window $T_v$ can be interpreted as the typical duration time of the event.

Since we are primarily concerned with events characterized by large $Q_2$ and $Q_4$ amplitudes, it seems logical to apply the VITA function to the $uv(t) = u(t).v(t)$ product time record. Since we want to retain the pattern of these burst events and to correlate them with the wall-pressure events, the contiguous VITA time record for $uv(t)$ and $p(t)$ are computed. Thus, two new records denoted by $p_v(t)$ and $uv_v(t)$ are generated for both the unfiltered and the filtered $u(t)$, $v(t)$ and $p(t)$ time records.

Figures 4.1 and 4.2 show the $uv(t)$ and the $uv_v(t)$ for the unfiltered and filtered data, respectively. The VITA time records show consistent detection of bursts in both cases. The cluster patterns are more clearly identified in the filtered data.

Similarly, figures 4.3 and 4.4 show $p(t)$ and $p_v(t)$ for the unfiltered and filtered data, respectively. The VITA time records again show consistent detection of bursts. The severely filtered pressure data still captures the intermittent events.

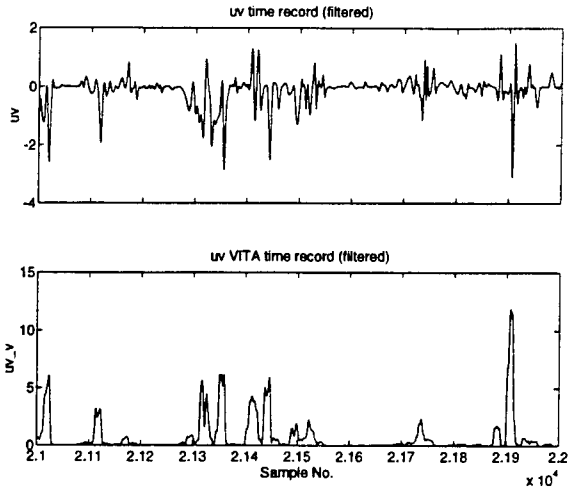


Figure 4.2: Sections of $uv(t)$ and $uv_v(t)$ (filtered) for $y+ = 30.9$.

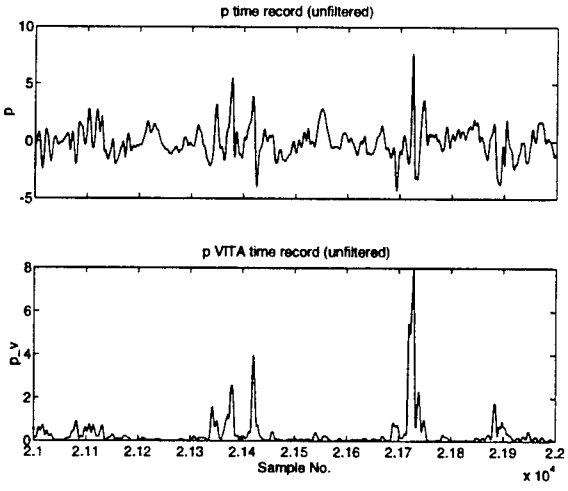


Figure 4.3: Sections of $p(t)$ and $p_v(t)$ (unfiltered) for $y+ = 30.9$.

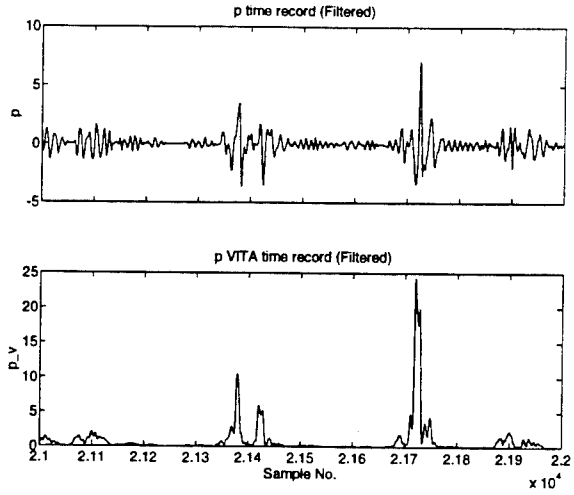


Figure 4.4: Sections of $p(t)$ and $p_v(t)$ (filtered) for $y+ = 30.9$.

## 4.2 Estimation of Convection Velocity

The convection velocity was previously estimated by computing the time delay between the $p_1(t)$ and $p_2(t)$ time records. Similar calculations were made using the VITA functions $p_{1_v}(t)$ and $p_{2_v}(t)$, respectively. The results for this correlation function computed from the unfiltered and filtered records are shown in figures 4.5 and 4.6, respectively. The convection velocities $U_c^+ = 16.5$ and $U_c^+ = 16.9$ were obtained and these compare favorably with those obtained from the original time data ($U_c^+ = 17.4, 16.5$).

It should be noted that the VITA functions are positive-definite, therefore the correlation between two of these functions will always be positive. Furthermore, if the correlation between two VITA functions generated from random time records is computed, a linear correlation will be obtained because of the zero padding. This is illustrated in figure 4.7 where the correlation between two independent VITA time records of the pressure were computed.

A normalization algorithm was incorporated that subtracted the linear correlation described above from the correlation function. The resulting function will be referred to as the Normalized Correlation of two positive definite functions $f_1(t)$ and $f_2(t)$ and will be denoted by $\mathrm{NC}(f_1(t), f_2(t))$. The NC function represents a relative measurement of the correlation and will be expressed in dB.

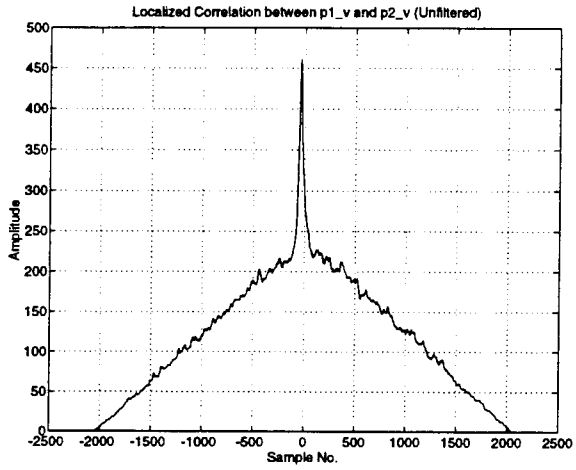


Figure 4.5: Localized correlation function between $p_{1_v}(t)$ and $p_{2_v}(t)$ (unfiltered) for hot-wire system at $y^+ = 30.9$.

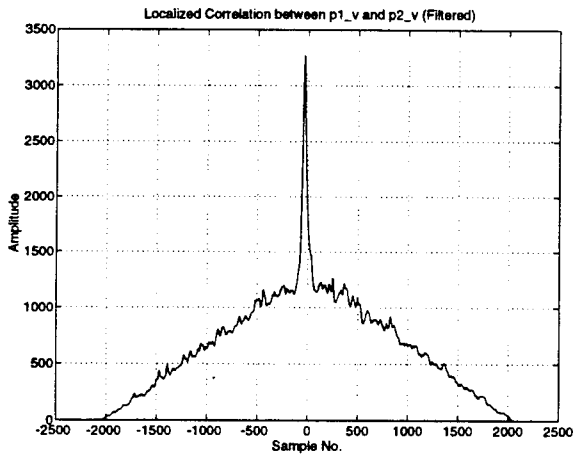


Figure 4.6: Localized correlation function between $p_{1_v}(t)$ and $p_{2_v}(t)$ (filtered) for hot-wire system at $y^+ = 30.9$.

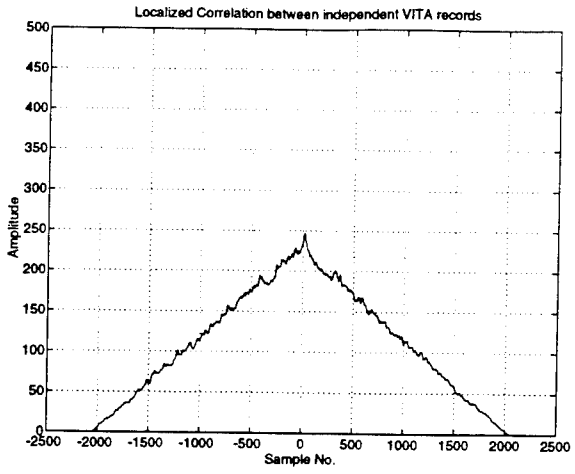


Figure 4.7: Localized correlation function between $p_{1_v}(t)$ for hot-wire system at $y^+ = 30.9$ and and $p_{1_v}(t)$ for hot-wire system at $y^+ = 64.9$ (unfiltered).

Figures 4.8 and 4.9 show the Normalized Correlation functions for the data presented in figures 4.5 and 4.6. Note that the filtered data shows higher correlation.

## 4.3 Correlation between Burst and Wall-Pressure VITA Functions

A normalized correlation function NC $(p_v(t), uv_v(t))$was computed for the $uv_v(t)$ and $p_v(t)$, where $p_v(t)$ is equivalent to $p_{1_v}(t)$ unless noted. These calculations were performed at 22 locations across the boundary layer. The correlations peaked at $y+ \approx 35$, were maintained within the region $y^+ < 300$, and then decreased to negligible magnitude outside the log-law region. The results for the unfiltered and filtered data for two locations are shown in figures 4.10 and 4.11, respectively. Again, the filter data show higher correlation. The correlation in the log-law region was not observed when using the $uv(t)$ and $p(t)$ time records.

It should be noted that, for both the unfiltered and filtered data, no time delay can be detected between the two VITA functions at the near-wall location $y^+ = 30.9$; while a significant time delay is observed at the location

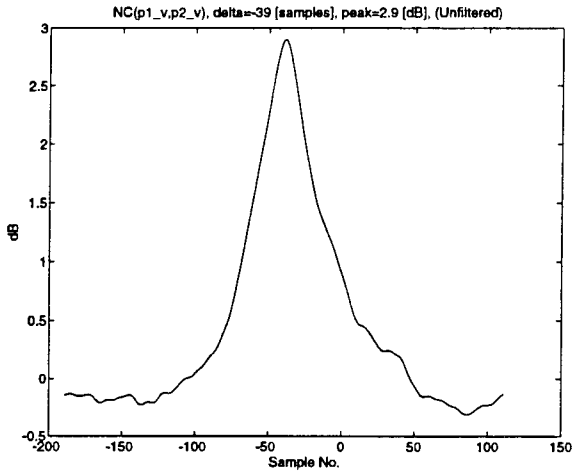


Figure 4.8: Normalized Correlation function between $p_{1_v}(t)$ and $p_{2_v}(t)$ (unfiltered) for hot-wire system at $y^+ = 30.9$.

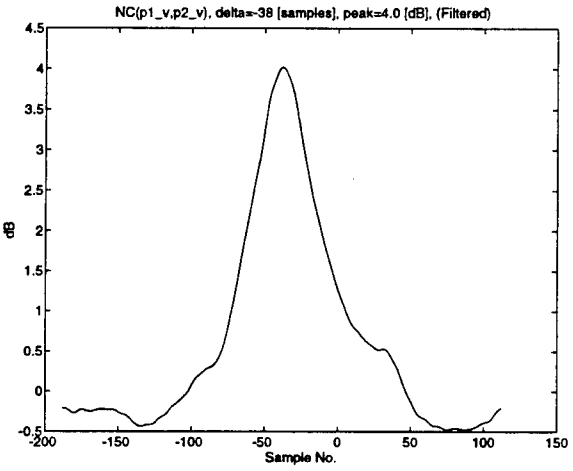


Figure 4.9: Normalized Correlation function between $p_{1_v}(t)$ and $p_{2_v}(t)$ (filtered) for hot-wire system at $y^+ = 30.9$.

$y^+ = 173.3$. This indicates that the organized motion burst mechanism extends to the log-law region and has a forward angle of inclination. The angle of inclination, calculated using the convection velocity and correlation results, was approximately 18 degrees. This value is consistent with the results of Snarski and Lueptow (cf. [5]).

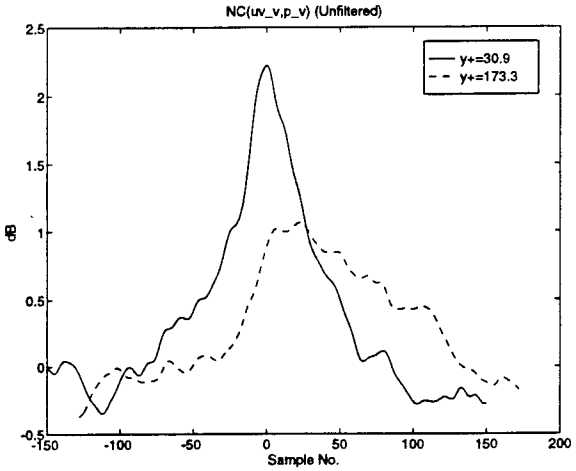


Figure 4.10: Normalized Correlation function between $uv_v(t)$ and $p_v(t)$ (unfiltered) for hot-wire system at $y^+ = 30.9$ and $y^+ = 173.3$.

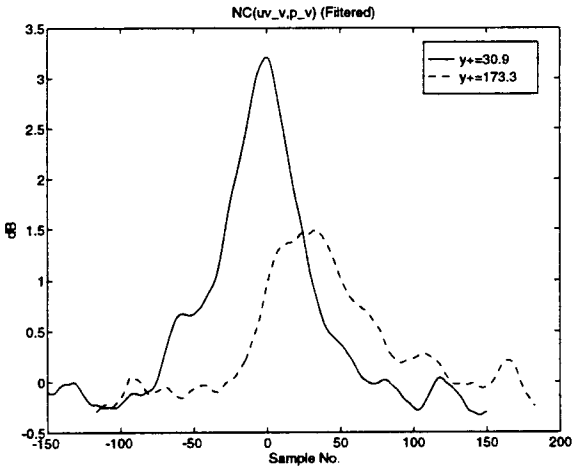


Figure 4.11: Normalized Correlation function between $uv_v(t)$ and $p_v(t)$ (filtered) for hot-wire system at $y^+ = 30.9$ and $y^+ = 173.3$.

# Chapter 5

# DETECTION OF CLUSTER PATTERNS

As previously discussed, the primary goal is to identify the wall-pressure signature pattern of the intermittent organized motion. Based on observations of the time records, the conjecture is made that the so-called cluster patterns of large amplitude $uv(t)$ events represent the organized motions while the $p(t)$ groupings represent the footprint of these structures. The results for correlation of clusters based on the VITA time records were presented and provided strong support for this hypothesis. However, it is often said that *correlation does not mean causation.* Therefore, a more detailed examination of these patterns is required. The first task is to identify the cluster patterns of both $uv(t)$ and $p(t)$ time records.

## 5.1 Review of Detection of Individual Events

Most methods for the detection of large amplitude intermittent events are based on the detection of events that exceed a threshold amplitude level. The peak events are windowed based on zero crossing and then ensemble averaged. For a prescribed threshold, typical statistical properties computed are: number of events, average duration of events and average time between events. (In most cases the number of events is simply the total time recorded divided by the average time between events.).

Karangelen (1991) (cf. [20]), Wilczynski (1992) (cf. [7]) and Kammeyer

Table 5.1: Higher moments for filtered and unfiltered data

| Events | Unfiltered | | Filtered | |
|---|---|---|---|---|
| | Skewness | Kurtosis | Skewness | Kurtosis |
| gaussian | 0 | 3.0 | - | - |
| $uv$ | $-1.8$ | 14.9 | -2.1 | 19.9 |
| $p$ | -0.05 | 4.3 | -0.07 | 10.5 |

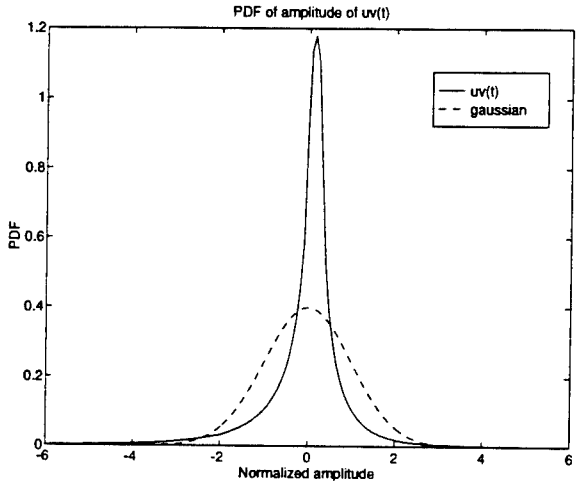


Figure 5.1: PDF of amplitude of $uv(t)$ F2 filtered time records at $y^+ = 30.9$.

(1995) (cf. [24]) computed the statistical properties of large amplitude events for both the turbulent and wall pressure time records, and compared these properties to gaussian statistics. Their findings can be briefly summarized as:

1. The amplitudes of these events have non-gaussian properties with distinct higher moments for both filtered and unfiltered data (see table 5.1 and figures 5.1 and 5.2):

2. Large amplitude events are more prevalent in turbulent and wall-pressure events than in gaussian data, as evidenced in the kurtosis data. Turbulent events are dominated by Q2 and Q4 events.

3. The times between peak events have log-normal distribution for gaussian data. To a first approximation, this pattern is also observed in the

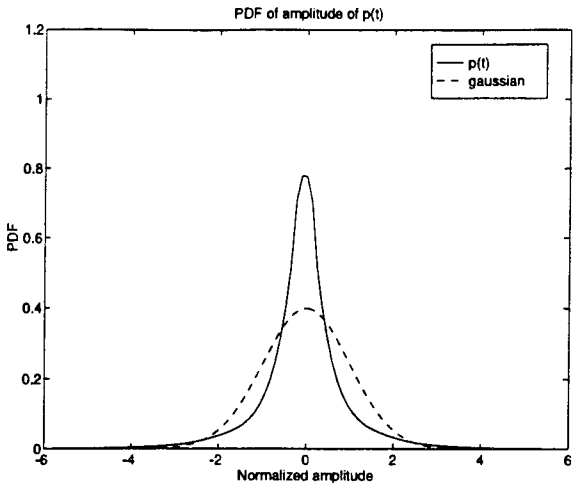


Figure 5.2: PDF of amplitude of $p(t)$ F2 filtered time records.

turbulent and wall-pressure data.

4. The relationship between the average time between events ($\overline{T}$) and threshold level $K$ can be approximated by $\log \overline{T} = f(K) \approx \alpha_0 + \alpha_1 K$.

For the detection of cluster patterns in the $uv(t)$ and $p(t)$ time records, peak detection of individual events is not necessarily beneficial. Furthermore, the strength of the wall-pressure signatures of turbulent events is not dependent on the amplitude of the burst-events but primarily on its spatial location. Therefore, separate threshold levels for contiguous burst-events and wall-pressure events are required but are not easily defined.

An algorithm is needed that captures the cluster pattern without prescribing a unique threshold level. This procedure must also try to identify those patterns that occur simultaneously in both the $uv(t)$ and $p(t)$ time records. The VITA function detection scheme was a first attempt at this task, however it provides a function rather than specific cluster locations and durations. These quantities are required for observing cluster patterns.

## 5.2 Localized Windowed Peak Detection

A new detection technique was developed that captures the cluster patterns of peak events independent of a threshold level. This technique is based on a Localized Windowed Peak Detection algorithm (LWPD).

The algorithm performs a recursive search of localized peak events throughout the time record and records their locations and durations. The only adjustable parameter of the algorithm is given by the window size $T_w$ that specifies the minimum distance between successive peaks. The algorithm is more computationally intense than the traditional peak level detection algorithm but surprisingly robust for a wide range of random-like time records.

The single parameter $T_w$ governs statistical properties such as number of events, average duration, and average time between cluster patterns. It is important to note that the number of cluster patterns detected by the LWPD algorithm is mainly governed by $T_w$ with weak dependence on the distinct features of the time record. This implies that for a prescribed $T_w$, the number of events detected by the algorithm in a gaussian time record and $uv(t)$ or $p(t)$ time records will be approximately the same. The locations and distinct patterns will be different. This feature of the LWPD algorithm might appear to be troubling, but with a little afterthought it has its benefits.

We take advantage of this characteristic of the LWPD algorithm by defining the same time window value $T_w$ for both $uv(t)$ and $p(t)$ time records. This insures conformity in number of events for both records. The selection of the optimal value of the time window is the major task. The criterion for optimal choice of $T_w$ is based on maximizing the correlation between concurrent events. The range for the window size is $40 \leq T_w^+ \leq 120$ ($50 \leq T_w \leq 150$ data samples). These bounds were established from extensive observations of the time records (for example, see figures 2.13 and 2.14). Figures 5.3 and 5.4 display the properties of the LWPD algorithm over a range of window sizes. The number of clusters, average duration and average time between clusters are presented. These data were computed from the $uv(t)$ time record, however, these results are universal for all records.

The value of $T_w^+ = 60$ was chosen for the equilibrium data based on numerous test cases. This choice resulted in the properties displayed in table 5.2. Using this window size, the results for a sample of the equilibrium $uv_w(t)$ and $p_w(t)$ time records are shown in figure 5.5. The duration and location of the cluster patterns in the pressure data were obtained by applying

Table 5.2: Properties of the LWPD algorithm for $T_w^+ = 60$

| | |
|---|---|
| Average number of clusters | 9 per 1000 $t^+$ units |
| Average time between clusters | 109 $t^+$ units |
| Average duration of a cluster | 48 $t^+$ units |

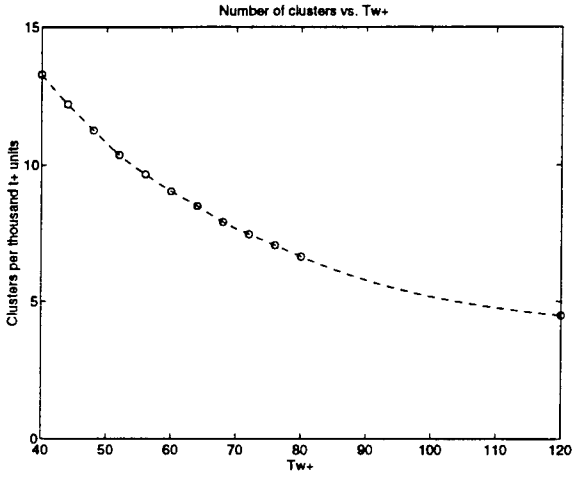


Figure 5.3: Number of clusters per thousand $t+$ units versus window size ($T_w+$). Computations based on the LWPD algorithm.

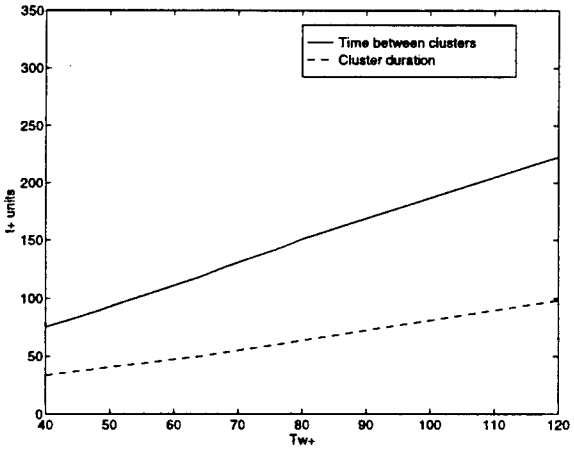


Figure 5.4: Time between clusters and Cluster duration in $t+$ units versus window size ($T_w+$). Computations based on the LWPD algorithm.

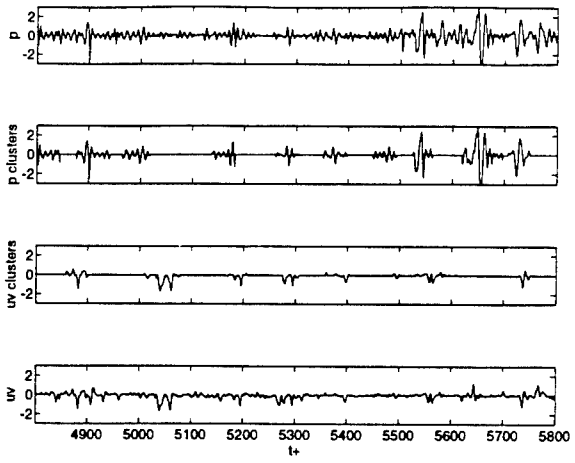


Figure 5.5: Detection of clusters from sections of $p_w(t)$ and $uv_w(t)$ time records using the LWPD algorithm ($y^+ = 30.9$).

the LWPD algorithm to the positive pressure peaks. The pressure samples outside the clusters were set to zero. Other options for the pressure time record were examined, however the positive pressure peaks produced the most meaningful results. The cluster patterns for the $uv_w(t)$ time records were also obtained using the LWPD algorithm based on negative peaks and setting to zero the sample points outside the clusters.

## 5.3 Results for Equilibrium Flow

The task is to identify the cluster patterns in the wall-pressure $p_{2_w}(t)$ and $p_{1_w}(t)$ time records that are signatures of the turbulent events contained in the $uv_w(t)$ time records. The ejection and sweep burst events (labeled Q2 and Q4 events) are contained in the $uv_w(t)$ time records and are of primary importance. Therefore, two new time records denoted by $\mathrm{Q2}_w(t)$ and $\mathrm{Q4}_w(t)$ will be generated. The $\mathrm{Q2}_w(t)$ time record includes only the $uv_w(t)$ sample points with $u_w(t) < 0$ and $v_w(t) > 0$. The $\mathrm{Q4}_w(t)$ includes only the $uv_w(t)$ sample points with $u_w(t) > 0$ and $v_w(t) < 0$. All other data points are set to zero in both cases. The corresponding cluster patterns will be labeled $p_{1_c}(t)$, $p_{2_c}(t)$,$uv_c(t)$, $Q2_c(t)$ and $Q4_c(t)$.

The application of the LWPD algorithm to filtered equilibrium data at

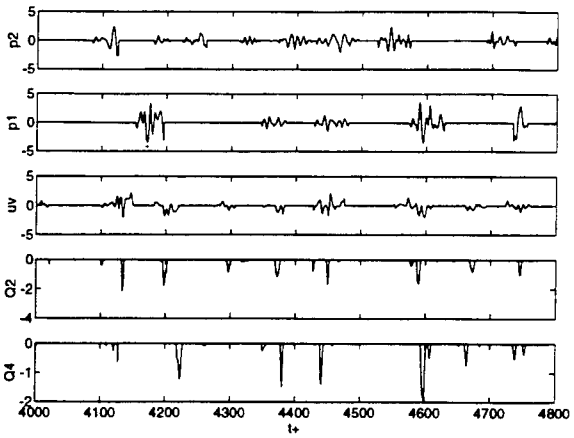


Figure 5.6: Sections of $p_{2_c}(t)$, $p_{1_c}(t)$, $uv_c(t)$, $\mathrm{Q2}_c(t)$ and $\mathrm{Q4}_c(t)$ time records ($y^+ = 30.9$).

the near-wall location generates cluster patterns as displayed in figures 5.6 and 5.7. These figures show the concurrent cluster patterns $p_{2_c}(t)$, $p_{1_c}(t)$, $uv_c(t)$, $\mathrm{Q2}_c(t)$ and $\mathrm{Q4}_c(t)$. For these results the LWPD algorithm was applied independently to the $p_{2_w}(t)$, $p_{1_w}(t)$, $uv_w(t)$, $\mathrm{Q2}_w(t)$ and $\mathrm{Q4}_w(t)$time records. From the limited data displayed in these figures it appears that the LWPD algorithm combined with the filtering techniques is successful in detecting contiguous cluster patterns that simultaneously occur in both turbulent flow and wall-pressure records.

The major contributions of the LWPD algorithm are to detect the locations of the cluster patterns and estimate their durations. The distinct features of the cluster patterns were examined by utilizing the correlation functions and conditional sampling techniques on the time records.

### 5.3.1 Correlations Between Cluster Time Records.

The $\mathrm{NC}(p_{1_{c_v}}, p_{2_{c_v}})$ function (figure 5.8) shows that $p_{1_c}$ and $p_{2_c}$ are highly correlated and therefore appear to detect concurrent events. The time delay (38 samples) between $p_{1_{c_v}}$ and $p_{2_{c_v}}$ is identical with those displayed in figures 4.8 and 4.9. The magnitude of the peak correlation is higher for this new method.

Despite this high correlation, it should be noted that there are distinct

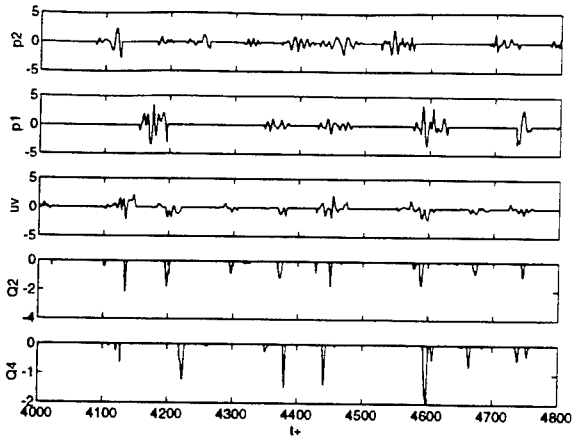


Figure 5.7: Sections of $p_{2_c}(t)$, $p_{1_c}(t)$, $uv_c(t)$, $Q2_c(t)$ and $Q4_c(t)$ time records ($y^+ = 30.9$).

Table 5.3: Proposed pairs and triplets of Q2 and Q4 events within each cluster

| | | | | |
|---|---|---|---|---|
| Q2 | $\longrightarrow$ | Q4 | | |
| Q4 | $\longrightarrow$ | Q2 | | |
| Q2 | $\longrightarrow$ | Q4 | $\longrightarrow$ | Q2 |
| Q4 | $\longrightarrow$ | Q2 | $\longrightarrow$ | Q4 |

cluster patterns in $p_{1_c}(t)$ and $p_{2_c}(t)$ that are not simultaneously observed in both time records (see figures 5.6 and 5.7).

The sequential patterns of the Q2 and Q4 events within each cluster can be examined from the computation of the correlation between the independently obtained $Q2_c(t)$ and $Q4_c(t)$ time records. These results are shown in Figure 5.9. The time delay with the smaller peak is $\Delta_1 \approx 18$ samples (14.4 $t^+$ units) while the time delay for the larger peak is $\Delta_2 \approx 14$ samples ($11.2t^+$ units). The occurrence of two peaks of different amplitudes and different time delays leads to a conjecture of possible patterns within each cluster. The pairs and triplets of Q2 and Q4 events sequentially detected by the sensors are proposed in table 5.3.

Independent confirmation of these sequential patterns can be obtained from the correlation of the $p_{1_c}(t)$ with the $Q2_c(t)$ time records. The Normal-

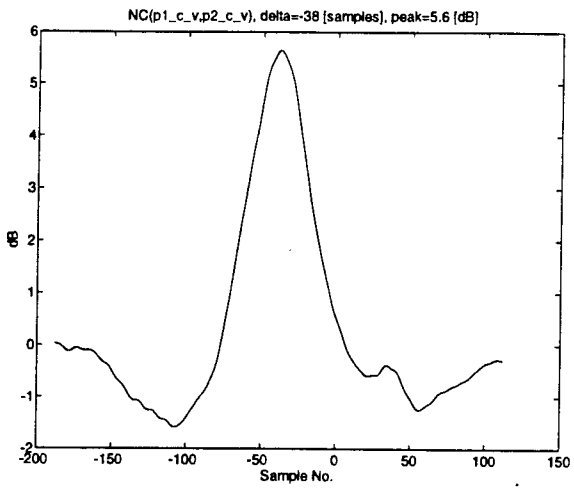


Figure 5.8: Normalized Correlation function between $p_{1_{c_v}}(t)$ and $p_{2_{c_v}}(t)$ $(y^+ = 30.9)$.

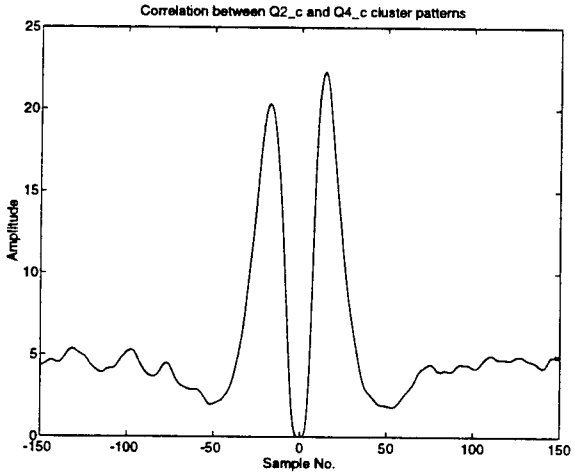


Figure 5.9: Correlation function between $\mathrm{Q2}_c(t)$ and $\mathrm{Q4}_c(t)$ $(y^+ = 30.9)$.

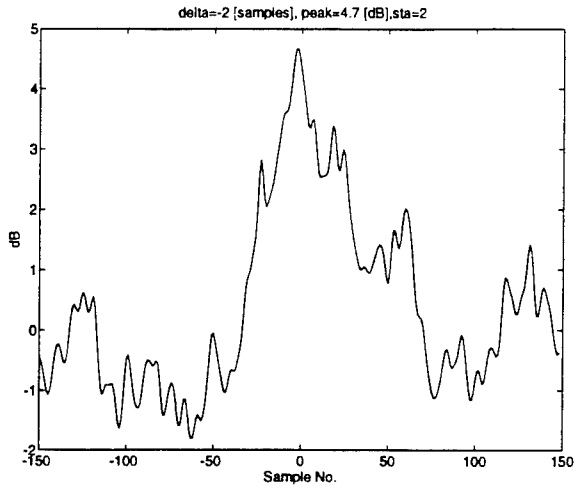


Figure 5.10: NC$(p_{1_c}^2(t), \mathrm{Q2}_c^2(t)$ function $(y^+ = 30.9)$.

ized Correlation function NC $\left(p_{1_c}^2(t), \mathrm{Q2}_c^2(t)\right)$ is shown in figure 5.10. The results indicate that the large amplitude pressure clusters are strongly correlated with Q2 events and have negligible time delay. Furthermore, the two minimums located at $\Delta_1$ (left) and $\Delta_2$ (right) time delays with respect to the central peak are indicative of Q4 events. These time delays are consistent with those shown in figure 5.9 which indicates that the probable time delays between Q2 and Q4 are Q2 $\xrightarrow{\Delta_2}$ Q4 and Q4 $\xrightarrow{\Delta_1}$ Q2.

Since positive pressure peaks correlate with Q2 events with negligible delay, the proposed alignment of pairs and triples can now be more explicitly defined as indicated in figure 5.11

### 5.3.2 Conditional Sampling Based on Cluster Locations.

The features of the cluster patterns can also be examined from conditional sampling based on the locations obtained from the LWPD algorithm. A rectangular window is centered around the detected location for each cluster. The windowed clusters are ensembled averaged over the original (filtered) time records.

The LWPD algorithm was applied to the Q2$(t)$ time records in order to determine the cluster locations based on negative Q2 peaks. Using these

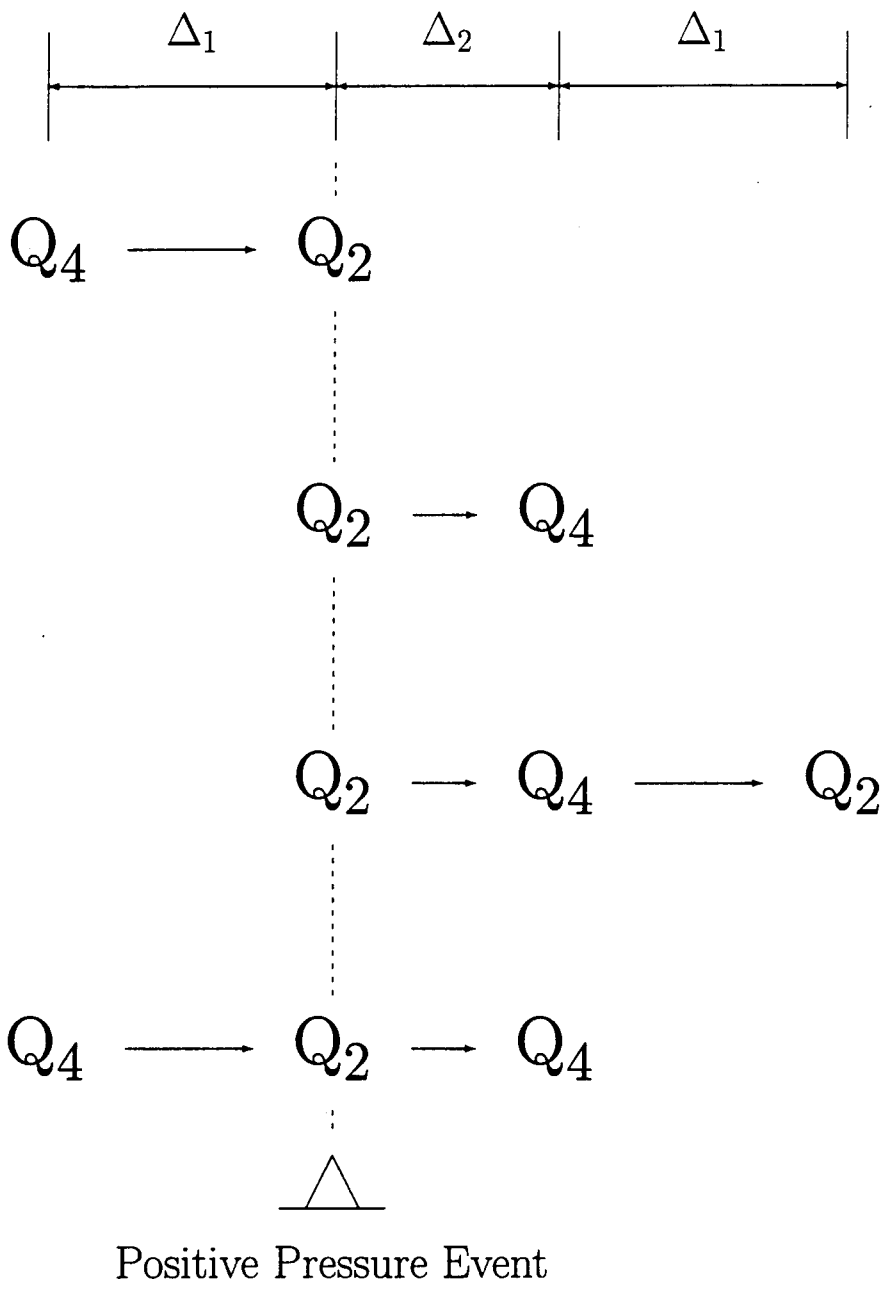


Figure 5.11: Alignment of combined Q2 and Q4 pairs and triplets within clusters.

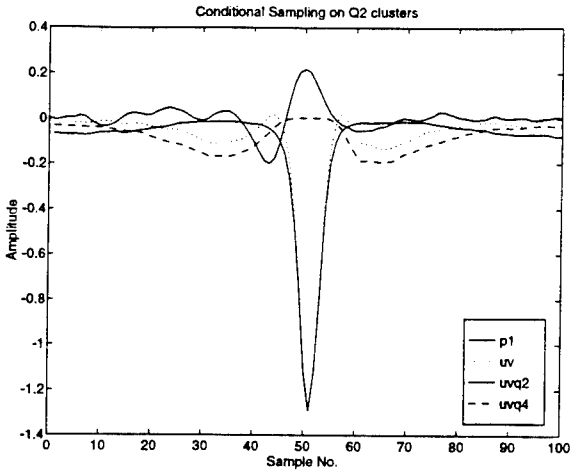


Figure 5.12: Conditional sampling of the $p_1(t)$, $uv(t)$, Q2$(t)$ and Q4$(t)$ time records based on the locations of Q2 clusters ($y^+ = 30.9$).

locations, the original (filtered) time records were ensembled averaged over the (1857) resulting clusters. Figure 5.12 displays these computations. These results are consistent with the conjectures made regarding the sequential patterns shown in figure 5.11 with the exception of the Q2 $\xrightarrow{\Delta_2}$ Q4 $\xrightarrow{\Delta_1}$ Q2 sequence. The time delays $\Delta_1$ and $\Delta_2$ are also confirmed. It should be noticed that the peak positive presure events were found to have good alignment with the detected Q2 peaks.

The LWPD algorithm was also applied to the Q4$(t)$ time record and the results are presented in figure 5.13. Even though the LWPD algorithm imposes the average number of clusters detected, the number of Q4 clusters (1832) is less than those obtained for Q2 clusters (1857). This implies that the Q4 $\xrightarrow{\Delta_1}$ Q2 $\xrightarrow{\Delta_2}$ Q4 is less likely to occur as compared to the other patterns. When comparing the ensemble averaged amplitudes of the Q2 and Q4 events from figures 5.12 and 5.13, it is evident that the amplitude of the Q2 events is larger than the amplitude of the Q4 events.

Our primary objective of this research is to use the pressure signatures for the detection of organized structures represented by patterns of Q events. Therefore, the final confirmation of a bidirectional relationship between wall-pressure and turbulent structures is required. The LWPD algorithm was uti-

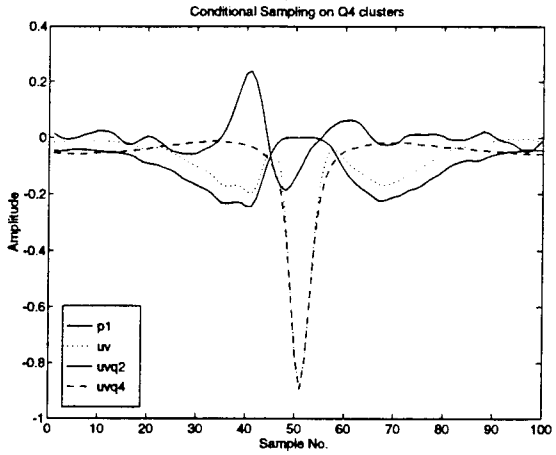


Figure 5.13: Conditional sampling of the $p_1(t)$, $uv(t)$, Q2$(t)$ and Q4$(t)$ time records based on the locations of Q4 clusters ($y^+ = 30.9$).

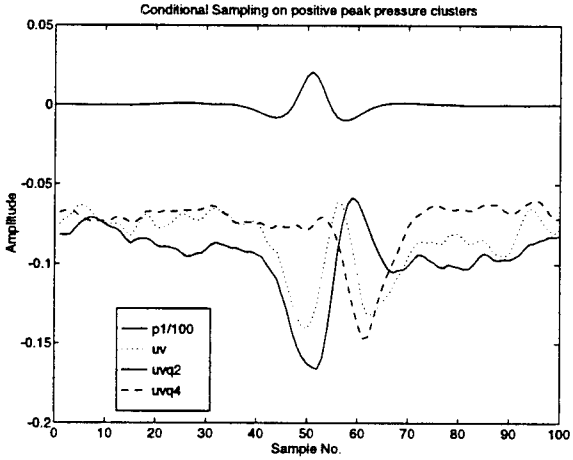


Figure 5.14: Conditional sampling of the $p_1(t)$, $uv(t)$, Q2$(t)$ and Q4$(t)$ time records based on the locations of positive peak pressure clusters ($y^+ = 30.9$).

lized to detect the cluster locations based on positive pressure peaks. Conditional sampling based on these locations (1863) was performed and the results are shown in figure 5.14. The most important result is that by conditionally sampling on pressure, Q2 events are aligned with the positive pressure peaks. By comparing the results of figures 5.12 and 5.14 it is concluded that a bidirectional relationship exists between positive pressure peaks and Q2 events. It should be noted that in previous investigations the phase jitter prevented the clear identification of this relationship between burst and wall-pressure events. These difficulties have been partially overcome by using the LWPD algorithm as well as an improved data acquisition system and higher sampling rates.

# Chapter 6

# SUMMARY AND DISCUSSION

The purpose of the research was two-fold: first, to confirm that large amplitude wall-pressure events are, in fact, footprints of organized active motions; and secondly, to develop detection algorithms that can capture the cluster patterns or groupings of these events.

The initial task was to acquire reliable experimental data that can be used for the investigation. Experiments were performed in a specially designed flow facility using a newly acquired VXI data acquisition system. The development of software drivers was very time consuming but the benefits justified the effort. Contiguous raw data of high quality were obtained with minimal errors due to background noise, phase distortion, and data-acquisition procedures. These databases on $u(t)$, $v(t)$ and $p(t)$ were acquired for both equilibrium and non-equilibrium flows at numerous locations across the boundary layer.

Numerous signal processing techniques were applied to the databases to investigate the research task. Wavelet filtering of the $u(t)$ and $v(t)$ time records proved to be successful in maintaining the distinct features of the near-wall intermittent burst events associated with turbulent production. Though this filtering might appear to essentially act as a high-pass filter, wavelet filtering is more refined because of its ability to maintain the integrity of localized events. The filtering of the wall-pressure time record required special consideration because it contains contributions from turbulent sources throughout the boundary layer. This necessitated a filtering algorithm with

significantly more reduction in the energy content. However, the features of the large amplitude events were still maintained.

A primary task of this investigation was to show explicitly the bi-directional relationship between turbulent and wall-pressure events. Extensive computations of the correlation between these time records were initially made to validate the integrity of the temporal records. These calculations were performed with both filtered and unfiltered data.

The convection velocity of the organized motion was estimated from time records generated by two spatially separated wall transducers. The phase relationship (time delay) between the turbulent structures located across the boundary layer and their wall-pressure footprints was also examined. These calculations were made using both, traditional methods based on the direct correlations of the original time records, and a new method based on the VITA function time records. Both methods produced consistent results, however, the VITA detection technique based on clusters of events was more successful in correlating $uv(t)$ and $p(t)$ events away from the wall and thus identifying the spatial extent of the organized motion.

The most challenging aspect of the research was to identify the distinct cluster pattern or grouping of burst events associated with the passage of organized structures. The LWPD detection technique was developed that performs a recursive search of localized peak events within a prescribed window and identifies the locations and durations of the clusters.

The LWPD algorithm created cluster time records of the groupings of the events with zero's between the clusters. Comparison of the original time record, VITA function time record, and cluster time record indicated that the locations and durations of the peak events were maintained in all the time records.

The computation of the convection velocity, based on the time delay obtained from the correlation of the time records of two streamwise wall-pressure transducers, showed consistent results for the three records. These results are shown in table 6.1.

Calculations based on correlation and conditional sampling techniques were used to examine the distinct pattern of events within the groupings. Sequential pairs and triplets of Q2 and Q4 events are postulated from these results. Furthermore, it appears that positive peaks in the wall-pressure are aligned with the Q2 events. Results using conditional sampling based on the LWPD algorithm for detection of cluster locations, confirmed this finding.

Table 6.1: Comparison of results on convection velocity of organized structures for equilibrium data

| time record | $U_c^+ = 16.9 \pm 0.05$ | | $U_c/U_0 = 0.68 \pm 0.02$ | |
|---|---|---|---|---|
| | Unfiltered | Filtered | Unfiltered | Filtered |
| Original | 17.4 (37) | 16.5 (39) | 0.70 | 0.66 |
| VITA | 16.5 (39) | 16.9 (38) | 0.66 | 0.68 |
| LWPD | 16.5 (39) | 16.9 (38) | 0.66 | 0.68 |

Bracketed numbers are time delays in sampled points.

The ensembled averaged data showed a bi-directional relationship between positive wall-pressure events and Q2 events within the clusters.

The LWPD algorithm has some unique features that make it promising for the development of adaptive techniques which can be utilized in the design of active control of turbulent flows. Further generic studies are required to examine the benefits and shortcomings of the LWPD algorithm. Enhancements resulting from these studies are expected.

# ACKNOWLEDGEMENTS

This work was supported by the Office of Naval Research with Dr. L. Patrick Purtell as scientific officer, under Grant # N00014-88-K-0141.

# Bibliography


[1] Robinson, S.K.," Coherent Motions in the Turbulent Boundary Layer," Ann. Rev. of Fluid Mech., vol. 23, pp. 601–639, 1991.

[2] Farabee, T. M. and Casarella, M.J., "Spectral Features of Wall Pressure Fluctuations Beneath Turbulent Boundary Layers," Phys. Fluids A, Vol 3, No. 10, pp. 2410–2420, 1991.

[3] Kim, J., "On the Structure of Pressure Fluctuations in Simulated Turbulent Channel Flow," J. Fluid Mech., No. 205, pp. 421–451, 1989.

[4] Wilczynski, V., Casarella, M.J. and Kammeyer, M., "A Comparison of Data on Intermittent Turbulent and Wall Pressure Events," ASME Winter Meeting, NCA-Vol 15, FED-Vol 168, 1993.

[5] Snarski, S. R., and Lueptow, R.M., "Wall Pressure and Turbulent Structures in a Turbulent Boundary Layer on a Cylinder in Axial Flow," Submitted to J. Fluid Mech., 1994.

[6] Morrison, J. F., Tsai, H.M., Bradshaw, P., "Conditional-sampling Schemes for Turbulent flow, based on Variable-interval time averaging (VITA) algorithm," Experiments in Fluids, Vol. 7, pp. 173–189, 1989.

[7] Wilczynski, V., *Organized Turbulent Structures and Their Induced Wall Pressure Fluctuations,* PhD Dissertation, The Catholic University of America, 1992.

[8] Daubechies, I., *Ten Lectures on Wavelets,* Society for Industrial and Applied Mathematics, 1992.

[9] Meneveau, C., "Analysis of Turbulence in the Orthonormal Wavelet Representation," J. Fluid Mech. No. 232, pp. 469–520, 1991.

[10] Farge, M. "Wavelet Transform and their Applications to Turbulence," Annu. Rev. Fluid Mech., pp. 395–457, 1992.

[11] Zubair, L., "Studies in turbulence using Wavelets Transformations for Data Compression and Scale Separation," Ph.D. Dissertation, Yale, 1993.

[12] Lewalle, J., "Wavelet Analysis of Experimental Data: Some Methods and Underlying Physics," 25th. AIAA Fluid Dyn. Conf., AIAA 94-2281, June 1994.

[13] Liandrat, J. and Moret-Bailly, F., "The Wavelet Transform: Some Applications to Fluid Dynamics and Turbulence," Eur. J. Mech. B/Fluids, vol. 9, No. 1, pp. 111–119, 1990.

[14] Press H., et. al., *Numerical Recipes in C,* Cambridge Press, 1992.

[15] Wark, C. E. and Nagib, H. M., "Experimental Investigation of Coherent Structures in Turbulent Boundary Layers," J. Fluid Mech., No. 230, pp. 183–200, 1991.

[16] Guezennec, Y., *Documentation of Large Coherent Structures associated with Wall Events in Turbulent Boundary Layers,* PhD Dissertation, Illinois Institute of Technology, 1985.

[17] Kaftori, D., *Structures in the Turbulent Boundary Layer and their Interaction with Particles,* PhD Dissertation, University of California, Santa Barbara ,1993.

[18] Kaftori D., et. al., "Funnel-shaped Vortical Structures in Wall Turbulence," Phys. Fluids, Vol. 6, No. 9, pp. 3035–3050, 1994.

[19] Motard, R.L. and Joseph, B., *Wavelet Applications in Chemical Engineering,* Kluwer Academic Publishers, July 1994.

[20] Karangelen, C. C., *Temporal and Spectral Features of Wall-Pressure Fluctuations Beneath a Turbulent Boundary Layer,* PhD Dissertation, The Catholic University of America, 1991.

[21] Bradshaw, P., "Turbulence: The Chief Outstanding Difficulty of our Subject, " Experiments in Fluids, No. 16, pp. 203–216, 1994.

[22] Bradshaw, P., " Inactive Motion and Pressure Pressure Fluctuations in Turbulent Boundary Layers", J. Fluid Mech., No. 30, pp. 241–258, 1967.

[23] Casarella, M.J., Penafiel, P., and Kammeyer, M., "Application of Wavelet-Filtering Techniques to Intermittent Turbulent and Wall-Pressue Events," Part I, Technical Report, The Catholic University of America, October 1994.

[24] Kammeyer, M., *An Experimental Investigation of Organized Turbulent Motions and Wall Pressure Fluctuations in Complex Flows,* PhD. Dissertation, The Catholic University of America, 1995, (to be published).

# Distribution List

Dr. L. Patrick Purtell
Office of Naval Research
S&T Division
800 North Quincy Street
Arlington VA 22217-5660

Dr. Spiro G. Lekoudis
Office of Naval Research
S&T Division
800 North Quincy Street
Arlington VA 22217-5660

Dr. Theodore M. Farabee
Carderock Division, Code 725
Naval Surface Warfare Center
Bethesda MD 20084

Dr. Richard M. Lueptow
Mechanical Engineering Dept.
Northwestern University
2145 Sheridan Road
Evanston IL 60208

Dr. William L. Keith
Code 2141
Naval Undersea Warfare Center
New London CT 06320

Dr. Candace E. Wark
Mech. & Aerospace Engr. Dept.
Illinois Inst. of Technology
10 West 32nd Street
Chicago IL 60616-3793

Dr. P.R. Bandyopadhyay
Weapons Tech/Undersea Systems
Naval Undersea Warfare Center
1176 Howell Street
Newport RI 02841-1708

Professor J.F. Morrison
Department of Aeronautics
Imperial College
Prince Consort Road
London, SW7 2BY UK

Professor Peter Bradshaw
Mechanical Engineering Dept.
Stanford University
Stanford CA 94305-3030

Professor Ron F. Blackwelder
Aerospace Engineering Department
University of Southern California
Los Angeles Ca 90089-1191

Dr. Vincent Wilczynski
U.S. Coast Guard Academy
15 Mohegan Avenue
New London CT 06320

Dr. Ronald Panton
Mechanical Engineering Dept.
University of Texas
Austin TX 78712

Professor R. Sreenivasan
Mason Laboratory
Yale University
New Haven CT 06520

Defense Technical (4 copies)
Information Center
Cameron Station
Alexandria VA 22304-6145

Dr. John Sullivan
Aerospace Science Lab
Purdue University
3 Purdue Airport
West Lafayette IN 47906-3371

Professor Dennis Bushnell
NASA-Langley Research Center
M/S 197
Hampton VA 23681

Professor John K. Eaton
Mechanical Engineering Dept.
Stanford University
Stanford CA 94305

Professor John Foss
Mechanical Engineering Dept.
Michigan State University
A-118 Research Complex - Engr.
East Lansing MI 48824

Professor Yann Guezennec
Mechanical Engineering Dept.
Ohio State University
206 W 18th Avenue
Columbus OH 43210